



Aerosol characterization and radiative properties over Kavaratti, a remote island in southern Arabian Sea from the period of observations

Piyushkumar N. Patel ^{a,*}, U.C. Dumka ^{b,**}, K.N. Babu ^a, A.K. Mathur ^a

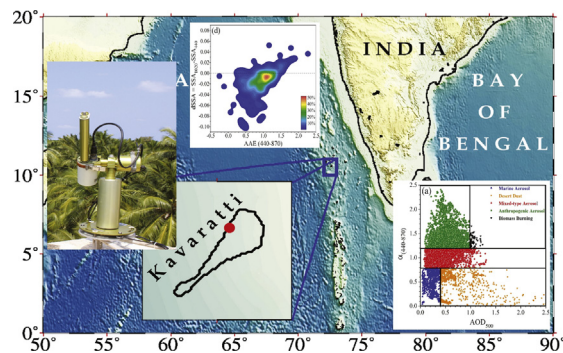
^a Calibration & Validation Division, Space Applications Centre, ISRO, Ahmedabad 380 015, India

^b Aryabhatta Research Institute of Observational Sciences, Nainital 263 001, India

HIGHLIGHTS

- Aerosol characterization carried out over Kavaratti, a remote island in southern Arabian Sea using a period of observations
- Large heterogeneity found in aerosol properties
- Advection plays a major role in modifying the aerosol properties.
- Increase in direct radiative forcing and atmospheric heating rate due to dust advection

GRAPHICAL ABSTRACT



ARTICLE INFO

Article history:

Received 19 December 2016

Received in revised form 18 April 2017

Accepted 22 April 2017

Available online xxxx

Editor: D. Barcelo

Keywords:

Aerosol types

Absorbing Ångström exponent

Southern Arabian Sea

Aerosol radiative forcing

Heating rate

ABSTRACT

Long-term measurements of spectral aerosol optical depth (AOD) using sun/sky radiometer for a period of five years (2009–2014) from the remote island location at Kavaratti (KVT; 10.56°N, 72.64°E) in the southern Arabian sea have been analysed. Climatologically, AODs decrease from October to reach maximum of ~0.6 (at 500 nm) in March, followed by a sudden fall towards May. Significant modulations of intra-seasonal timescales over this general pattern are noticed due to the changes in the relative strength of distinctively different sources. The corresponding changes in aerosol inversion parameters reveal the presence of coarse-mode aerosols during spring and fine-mode absorbing aerosols in autumn and winter months. An overall dominance of a mixed type of aerosols (~41%) with maximum in winter (~53%) was found via the AOD₅₀₀ vs. Ångström exponent ($\alpha_{440-870}$) relationship, while biomass-burning aerosols or thick urban/industrial plumes contribute to ~19%. Spectral dependence of Ångström exponent and aerosol absorbing properties were used to identify the aerosol types and its modification processes. Based on air mass back trajectory analysis, we revealed that the advection of aerosols from Indian subcontinent and western regions plays a major role in modifying the optical properties of aerosols over the observational site. The shortwave aerosol direct radiative forcing estimated via SBDART model ranges from -11.00 W m^{-2} to -7.38 W m^{-2} , -21.51 W m^{-2} to -14.33 W m^{-2} and 3.17 W m^{-2} and 10.0 W m^{-2} at top of atmosphere, surface and within the atmosphere, respectively. This atmospheric forcing translates into heating rate of $0.62\text{--}1.04 \text{ K day}^{-1}$. Furthermore, the vertical profiles of aerosols and heating rate exhibit significant increase in lower (during winter and autumn) and mid troposphere (during spring). This may cause serious climate implications over Kavaratti with further consequences on cloud microphysics and monsoon rainfall.

© 2017 Elsevier B.V. All rights reserved.

* Corresponding author.

** Correspondence to: U. C. Dumka, ARIES, Manora Peak, Nainital 263001, Uttarakhand, India.

E-mail addresses: piyushether@gmail.com (P.N. Patel), dumka@aries.res.in, ucdumka@gmail.com (U.C. Dumka).



1. Introduction

Atmospheric aerosols significantly modulate the radiation budget, cloud properties, atmospheric thermodynamics and overall climate of Earth-atmosphere system (IPCC, 2007). The rapid economic growth and budding energy demands, drastically increase the aerosol emission and their possible local/regional and global climate impacts, especially over the South Asia, which make essential to characterize the aerosols over both land and ocean (Satheesh et al., 2006a; Yoon et al., 2012, 2014; Moorthy et al., 2013). Despite the progress achieved in past few decades in understanding the radiative effects of aerosols, still significant uncertainties persist in the global climate studies due to inadequate understanding of the spatio-temporal heterogeneity in optical and physical properties of aerosols and their complex nonlinear interaction with atmospheric constituents (Boucher et al., 2013). Thus, it is important to improve the aerosol characterization with an adequate knowledge of its properties (physical, chemical and optical) and their impact on regional as well as global climate change with high spatial and temporal resolutions (Dey and Di Girolamo, 2010; Lodhi et al., 2013; Tiwari et al., 2015). Moreover, the investigation of aerosols over oceans are important to understand their anthropogenic and natural impacts as well as their contribution in estimation to radiative forcing (e.g., Haywood et al., 1999; Moorthy et al., 2009; Kaskaoutis et al., 2010, 2011). However, the large spatio-temporal variability and limited measurements of aerosol properties over oceanic regions hamper to understand their impacts on weather and hence climate change (Smirnov et al., 2009). Due to these reasons, the oceanic regions around Indian subcontinent have always been the subject of importance for extensive investigation through various experimental campaigns.

Indian subcontinent and its surrounding oceanic regions are considerably influenced by the long-range transport of aerosols (e.g., Ramanathan et al., 2001; Niranjan et al., 2007; Lawrence and Lelieveld, 2010; Patel and Shukla, 2015). Satellite observations showed that the transport of aerosols from the Asian continent to the adjoining oceans increases from winter (December–February) to pre-monsoon (March–May) and maximize during the summer monsoon season (June–September) (Nair et al., 2005). The Arabian Sea (AS) region has a unique weather pattern because of the varying atmospheric dynamics driven by the contrasting monsoons with its associated seasonal wind reversal. It is a location, where the pristine air masses from the Southern Indian Ocean and the polluted air from Asia meet during winter and spring season, providing a very interesting area for aerosol studies (e.g. Ramanathan et al., 2001; Kalapureddy et al., 2009; Kaskaoutis et al., 2010). Detailed investigations on the aerosol characterization over the AS were conducted during the Indian Ocean Experiment (INDOEX) (Ramanathan et al., 2001), the Arabian Sea Monsoon Experiment (ARMEX-I and ARMEX-II) (Vinoj and Satheesh, 2003; Babu et al., 2004; Moorthy et al., 2005) and the Integrated Campaign for Aerosols, gases and Radiation Budget (ICARB) (Moorthy et al., 2008). During summer monsoon, large sea-salt contribution to the aerosol optical depth (AOD) over the Southern AS is directly associated with stronger sea-surface winds (Satheesh et al., 2006b). During the pre-monsoon, intense plumes of mineral dust originating from the West Asian Deserts engulf almost the entire Arabian sea and reach at least up to the west coast of Peninsular India (e.g. Nair et al., 2005; Mishra et al., 2010; Patel and Shukla, 2015), causing a large impact to the radiative forcing in these regions (e.g. Satheesh et al., 2006a). On the contrary, the advection of continental polluted aerosols from Indian subcontinent, aided by favourable air mass during the winter season, perturb the pristine oceanic environments (Moorthy and Satheesh, 2000; Li and Ramanathan, 2002 and reference therein), which reduce the diurnal mean surface downwelling solar flux by about 15 to 35 W m⁻² (Ramanathan et al., 2001). Notwithstanding the large number of new findings, all these campaigns have been limited in their temporal coverage, the longest of these being the ICARB and as such, providing only a short sample that is subjected to temporal variations associated with the synoptic

and meteorological variables (Beegum et al., 2008). A few reports, available based on the extensive cruise measurements, are mostly season-specific or species specific and mostly serve as case studies. They are limited to a given season of the year and covered a very large oceanic region with embedded heterogeneity. Consequently, the spatial variability is coupled with the temporal variabilities. Though, the conclusion drawn from those papers (e.g., Vinoj and Satheesh, 2003; Moorthy et al., 2005, 2008; Kedia and Ramachandran, 2008a, b; Kalapureddy et al., 2009; Kaskaoutis et al., 2010 and reference therein) are valuable and suggestive but suffering from the above limitations. Therefore, long-term measurements of aerosol properties from the small island located in far oceanic regions, under the influence of populated and industrialized diverse continental landmass, provides a platform to define the impacts from different source regions, aided by favourable air-mass types in perturbing the rather oceanic environments through long-range transport (Moorthy and Satheesh, 2000; Li and Ramanathan, 2002; Moorthy et al., 2003). The only study has been carried out is the all-seasons aerosol characterization in the Southern Arabian Sea by Satheesh and Moorthy (2000) and Vinoj et al. (2010) based on extensive multi-year data from the island station Minicoy. To continue this study, the observations from a new remote island site over Kavaratti (KVT), Lakshadweep in southern AS developed under the calibration and validation (CAL-VAL) program of Space Applications Centre (SAC), Indian Space Research Organization (ISRO) (Shukla et al., 2013; Patel and Shukla, 2015; Patel et al., 2016) has been analysed.

The current work examines the aerosol characteristics using 5-years of continuous data (constrained by the weather conditions) from a fixed location, which offers insights into the aerosol climatological features and important inputs for the regional aerosol model. This paper scrutinizes the optical and radiative properties of AS aerosols using long-term continuous measurements obtained from the island station Kavaratti located in the Lakshadweep Archipelago in the southern AS, close to southwest edge of the Indian subcontinent (see Fig. 1). The analysis utilizes the sun/sky radiometer retrievals from October to May for five years (2009–2014) in order to study the temporal variations of aerosols, dominant aerosol types based on correlation between aerosol optical properties and modification processes in the atmosphere. The aerosol transport pathways and source identifications using Hybrid Single Particle Lagrangian Integrated Trajectory (HYSPLIT; Draxler and Rolph, 2016) model are also examined along with columnar and vertical aerosol direct radiative forcing (ADRF) and atmospheric heating rate (HR) using the Santa Barbara DISORT Atmospheric Radiative Transfer (SBDART; Ricchiazzi et al., 1998) model. The results are specifically important to understand the impacts of continental aerosols over oceanic environments and their implications to regional radiation budget.

2. Experimental site details

2.1. Observational site

Continuous measurements of columnar spectral AODs were carried out at Kavaratti (KVT; Fig. 1), the administrative capital of the Union Territory of Lakshadweep islands, a chain of islands spread from 8°N to 14°N and 71°E to 74°E in the southern AS. The island KVT lies 360 km off the coast of Kerala state in the Indian subcontinent at 10.57°N 72.64°E, and is located between Agatti island on the west and Andrott island on the east. Maximum length of the island is 5.8 km and width is 1.6 km. The total geographical area is ~4.22 km² and has population of about 11,201 (census 2011), with a growth rate of 10.78% during the last decade. The northwest side of the island is covered with the lagoon area having a length of about 6 km and area of ~4.96 km². The measurements were carried out on the terrace of the CAL-VAL laboratory (10.55°N; 72.60°E; marked as a red dot in the Fig. 1) building at about 12 m above the ground level, established under the CAL-VAL program (Shukla et al., 2013). The site located in the southern tip of the AS near to Indian subcontinent and it opens to

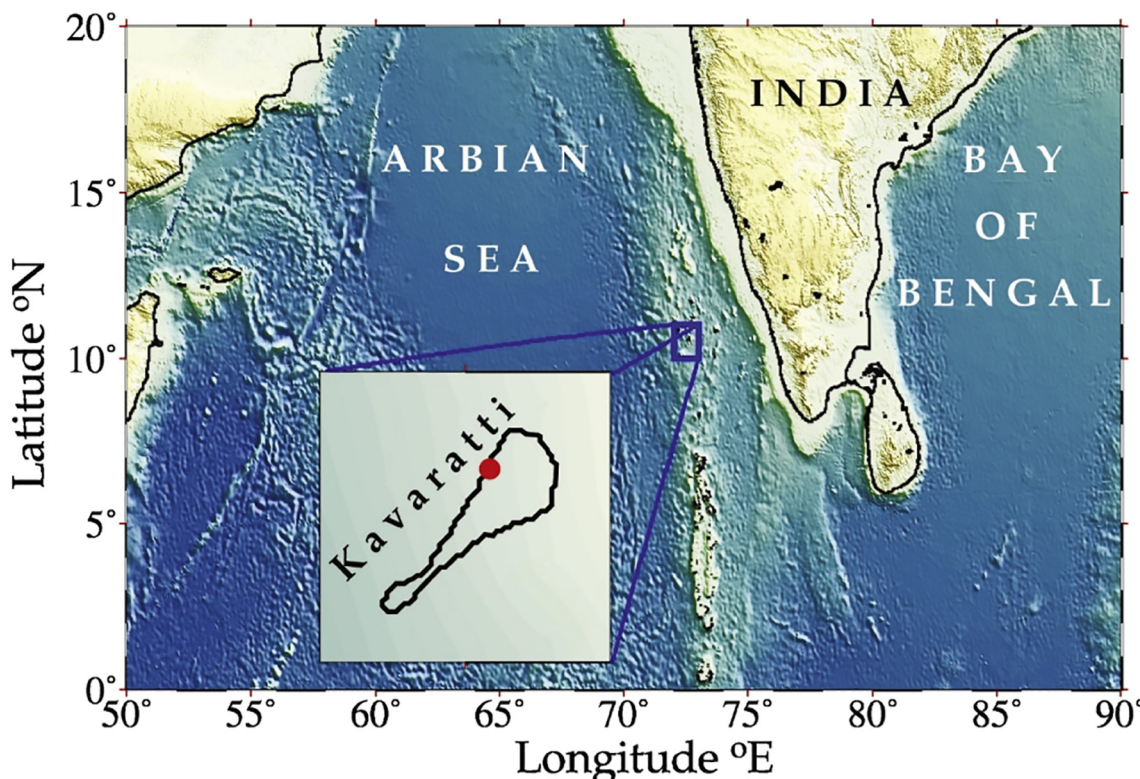


Fig. 1. The location of Kavaratti Island situated in the Lakshadweep Archipelago in the southern Arabian Sea. The red solid circle shows the meteorological laboratory at Kavaratti.

the arid regions in the west side. Therefore, the site is influenced by anthropogenic continental aerosols from the Indian subcontinent, desert dust from the western deserts and maritime aerosol from the AS, which are seasonally and intra-seasonally varying due to variation in hydrological cycle and movements of Inter-Tropical Convergence Zone (ITCZ; Kaskaoutis et al., 2015). The island is free from the industrial activities and characterized by dense forest and vast water bodies. Thus, it provides a clean marine platform for long-term measurements of aerosols over AS to study the background aerosol and influence of long-range transport.

2.2. Local meteorology

The station experiences a typical tropical climate with extensive rainfall. The local meteorological parameters such as temperature, relative humidity, wind speed and wind direction along with rainfall were obtained from met buoy and disdrometer, respectively, to understand the local meteorology over the measurement station (Shukla et al., 2013). The annual distribution of climatological mean monthly total rainfall is shown in Fig. 2a. The distribution shows negligible rainfall during January–March, with a gradual increase reaching maximum values by August (~780 mm). This persists till October with varying intensities, thereafter gradually decrease towards December. The climatological monthly mean of ambient temperature and relative humidity (RH) during the study period is plotted in Fig. 2(b–c). The mean maximum and minimum temperatures are in the range of 28.05–32.08 °C and 26.41–28.78 °C, respectively, with a hottest period during March–May. The averaged meteorological features revealed relatively low RH (<80%) from December to May, and high RH during June–November. The present study focuses on three seasons, autumn (October–November), winter (December–February) and spring (March–May). For remaining season of summer (June–September), the number of data points was less because of the adverse sky conditions associated with

extensive monsoon rainfall and the prevailing very high RH, which construct unfavourable environments for the CIMEL measurements.

The winds are crucial for the study of aerosol characterization and plays a very critical role on the monsoon circulation over Indian region (Moorthy and Sathesh, 2000; Sathesh et al., 2006a). The climatological mean seasonal wind pattern over the island is shown in Fig. 2(d–g). The color gives the magnitude of wind speed (in m s^{-1}). The weak ($<6 \text{ m s}^{-1}$) north-easterly winds during winter from the Indian subcontinent brings dry air mass, which may possess a large fraction of anthropogenic aerosols (Vinoj et al., 2008; Patel and Shukla, 2015). The winds are rather weak ($<4 \text{ m s}^{-1}$) and fluctuating between two extremes during autumn which is dominated by north-easterlies and easterlies. The transition of winds in spring is dominated by the northwesterly winds, carrying dust from the arid/semi-arid areas in Saharan and Arabian Peninsula (Kalapureddy and Devara, 2010; Kaskaoutis et al., 2010; Patel and Shukla, 2015). The strong westerly winds in summer following the onset of Indian summer monsoon, is significantly influence the regional climate with the dominance of marine components.

3. Measurements and methodology

3.1. Columnar aerosol measurements

Ground-based measurements of columnar aerosol properties were carried out over KVT Island using an automatic sun/sky radiometer (CIMEL CE-318). The five years of observations from October 2009 to May 2014 are analysed in the current study, since during June–September, the instrument stopped its operation due to the presence of dense clouds and extreme weather conditions. The CIMEL sun/sky radiometer measures the direct sun irradiance and diffuse sky-radiance at eight spectral bands centered at 340, 380, 440, 500, 670, 870, 940 and 1020 nm and 440, 670, 870 and 1020 nm, respectively. The measurements at 940 nm are used for the estimation of columnar water vapor content (WVC) and the remaining spectral bands are used to retrieve

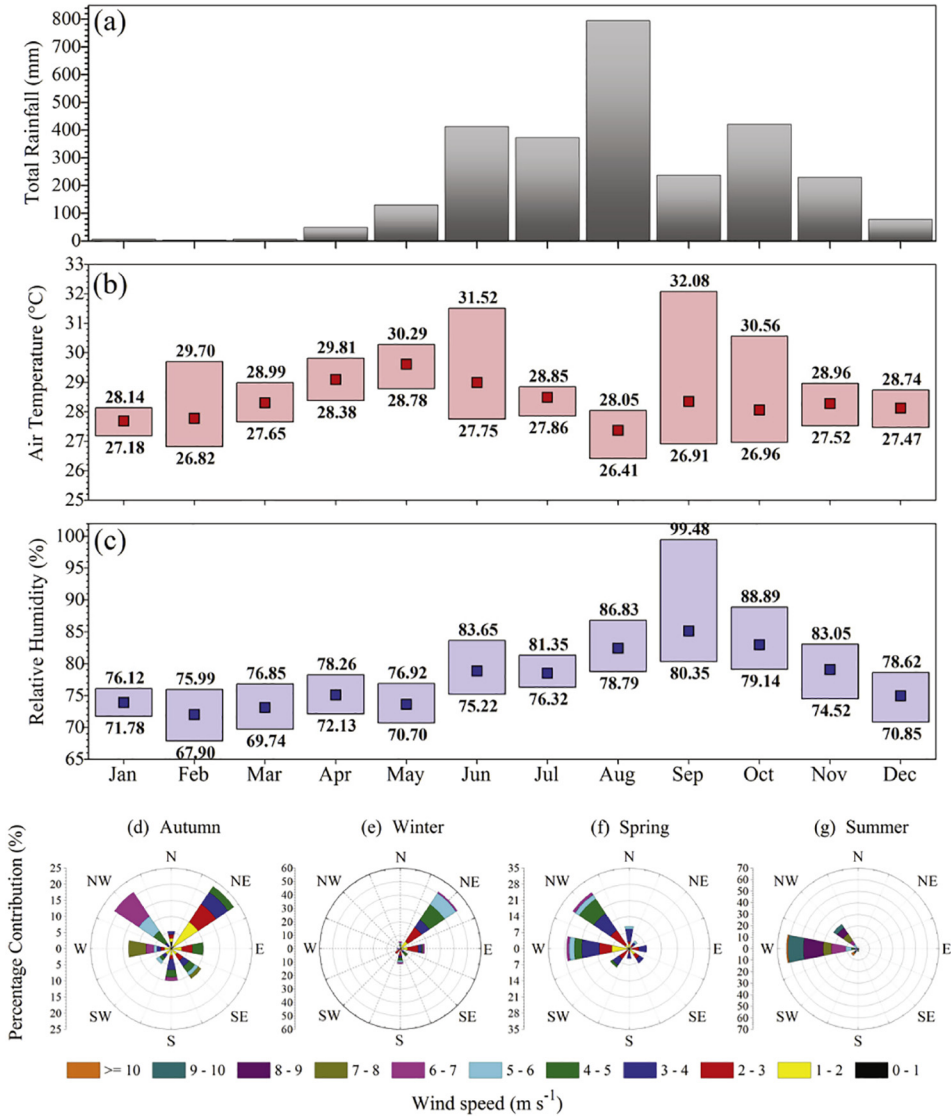


Fig. 2. The climatological distribution of (a) total rainfall, a monthly mean of (b) air temperature (in °C) and (c) relative humidity (in %) describes as a floating bars and the square in the bar represents the monthly mean values. (d–g) wind-rose plots describe the percentage contribution of seasonal variation of wind direction and wind speed over the period 2009–2014 at Kavaratti.

the columnar AOD. The filters used in the sun/sky radiometer are narrow bands with bandwidth of 10 nm except for 340 and 380 with bandwidth 2 nm. On the other hand, sky almucantar radiances from principal plane measurements are used to retrieve the optical and microphysical properties of aerosols such as Single Scattering Albedo (SSA), Asymmetry parameters (g), Volume Size Distribution (VSD) and refractive index. The measurement schedule for this instrument broadly consists of direct sun measurements every 15 min, and diffuse sky measurement at every 30 min. Triplets of sun measurements are performed at 20 s interval for cloud screening. Further details about the instrument characteristics and aerosol retrievals are given elsewhere (Estellés et al., 2012; Patel et al., 2016). The AOD, Ångström exponent (α) and WVC are retrieved for each scan under the clear-sky, while the inversion parameters are given on daily-mean basis.

Besides spectral AOD, α and its spectral dependence, an inversion algorithm can provide valuable information combining the direct sun and diffuse sky radiance measurements. In contrast to AERONET and SKYNET inversion algorithm, we have used a new open source package [ESR.pack; (Estellés et al., 2012)], which is based on Skyrad.pack (version 4.2) algorithm used in SKYNET. The ESR.pack has been modified and adapted for application to CIMEL CE-318 sun/sky radiometer. It is

a combination of two basic modules i) *Sunrad*, for the retrieval of direct sun products (e.g. AOD, α and WV) from the solar extinction measurements and ii) *Skyrad*, a modified version of Skyrad.pack version 4.2 (Nakajima et al., 1996; Kobayashi et al., 2010), to invert the sky radiance to obtain other aerosol characteristics such as phase function, VSD ($dV(r)/dlnr$), SSA, g and refractive index. In addition, the basic Smirnov et al. (2000) cloud screening algorithm was also implemented in order to assure the data quality and avoid cloud contamination. Details about ESR algorithm, methodology, uncertainties, calibration and intercomparison with the AERONET and SKYNET are presented elsewhere (Campanelli et al., 2004, 2007; Estellés et al., 2012; and references therein).

3.2. Ångström exponent and its derivatives

AOD and α are the two most crucial parameters to understand aerosol burden in the atmospheric column. α can be calculated from the Ångström power law given by Ångström (1964),

$$\tau_\alpha(\lambda) = \beta \lambda^{-\alpha} \quad (1)$$

where λ is the wavelength in micrometres, τ_a is measured AOD for the wavelength λ , α is Ångström exponent, and β is turbidity coefficient that is equal to columnar AOD at $\lambda = 1 \mu\text{m}$. α depends on the size distribution of aerosols, with higher value ($\alpha > 1$) indicating an enhancement of accumulation-mode aerosols and lower value ($\alpha < 1$) indicating enhancement of coarse-mode aerosols (Eck et al., 1999, 2010). Multimodal size distribution in the column introduces the uncertainty in the Eq. (1) for a wide range of wavelengths due to the different types of particles transported from different emission sources. Taking the logarithms at both sides of Eq. (1) yields:

$$\ln \tau_\lambda = -\alpha \ln \lambda + \ln \beta \quad (2)$$

For two different wavelengths (λ_1 and λ_2), α is given by

$$\alpha = -\ln(\tau_{\lambda_1}/\tau_{\lambda_2})/\ln(\lambda_1/\lambda_2) \quad (3)$$

where, τ_{λ_1} and τ_{λ_2} represent the AOD at two wavelengths λ_1 and λ_2 . This equation assumes that α is invariant in the spectral range λ_1 to λ_2 . This assumption is valid only when the particle size distribution in the vertical column follows an inverse power law (Beegum et al., 2009). A more precise empirical relationship between aerosol extinction and wavelength is obtained with a second-order polynomial fit (Eck et al., 1999; Kaskaoutis and Kambezidis, 2006) as

$$\ln \tau_\lambda = \alpha_2 (\ln \lambda)^2 + \alpha_1 (\ln \lambda) + \alpha_0 \quad (4)$$

where α_0 , α_1 and α_2 are constants that can be obtained from the sun/sky radiometer measurements. The coefficient α_2 accounts for a curvature often observed in sun-photometry measurements. This curvature can be an indicator of the aerosol particle size, with negative curvature indicating aerosol size distribution dominated by fine mode and positive curvature indicating size distribution with significant contribution by the coarse mode aerosols (Schuster et al., 2006).

3.3. Aerosol inversion products

Besides spectral AOD, α and its spectral dependence, an inversion algorithm can provide valuable information combining the direct sun and diffuse sky-radiance measurements. The column-integrated aerosol VSD ($dV(r)/dlnr$) is one of the crucial parameter for understanding the aerosol scattering processes and radiative impact (Sinha et al., 2013). VSD has been estimated at 22 radius bins ranging from 0.05 to $10 \mu\text{m}$ and exhibits bimodal distribution that can be characterized by the sum of two log-normal distributions (Seinfeld and Pandis, 1997).

$$\frac{dV(r)}{dlnr} = \sum_{i=1}^2 \frac{C_{v,i}}{\sqrt{2\pi\sigma_i^2}} \exp\left[-\frac{(\ln R - \ln R_{v,i})^2}{2\sigma_i^2}\right] \quad (5)$$

where, $C_{v,i}$ denotes the particle volume concentration, $R_{v,i}$ is the volume geometric mean radius, and σ_i is the standard deviation. In addition to VSD, the inversion algorithm provides the spectral SSA and ASY at four wavelengths (440, 675, 870 and 1020 nm), which are the important parameters to understand the absorption/scattering nature of particles. Additionally, the spectral absorption optical depth (AAOD) has been computed from the extinction AOD and SSA following previous studies (i.e. Bergstrom et al., 2007; Russell et al., 2010; Dumka et al., 2014), as:

$$\text{AAOD}(\lambda) = [1 - \text{SSA}(\lambda)] \times \text{AOD}(\lambda) \quad (6)$$

AAOD provides useful information about the absorbing optical properties of aerosols in the atmospheric column. Using the Ångström power law ($\text{AAOD}(\lambda) = K\lambda^{-\text{AAE}}$), where K correspond to the absorbing aerosol loading, the absorption Ångström exponent (AAE) and extinction Ångström exponent (EAE) have been computed by the negative slope of the fitted line of the natural logarithm of spectral variations in

AAOD and extinction aerosol optical depth (EAOD), respectively (Russell et al., 2010), which is analogous to the Ångström relationship (Ångström, 1964). These quantities are crucial to identify the particle size and characterize the dominant particle type or optical mixture (Giles et al., 2011).

3.4. Vertical aerosol measurements

In addition to ground based measurements, the vertical distribution of extinction coefficient is obtained from Cloud-Aerosol Lidar with Orthogonal Polarization (CALIOP) on-board the satellite CALIPSO (Winker et al., 2009) to examine the vertical distribution of aerosol and its impact on ADRF and atmospheric HR (Srivastava and Ramachandran, 2013). The extinction coefficients at 532 nm were obtained from the CALIOP level-2 version-3 data with 5-km horizontal resolution. Young and Vaughan (2009) used Hybrid Extinction Retrieval Algorithm (HERA) to derive the extinction coefficients, where the estimated measurement uncertainty in CALIOP derived aerosol extinction profiles is about 40%. The method by Misra et al. (2012) was employed to extract extinction profiles influenced by clouds. The monthly-mean profiles are obtained by averaging all the available profiles from CALIOP tracks within a spatial window of $1^\circ \times 1^\circ$ around the study region due to low orbit repetitiveness and narrow swath of CALIOP.

3.5. Estimation of ADRF and atmospheric heating rate

The ADRF at the top of the atmosphere (TOA) and surface (SFC) defines the net change in radiative flux caused by atmospheric aerosols, which is:

$$\Delta F_{\text{TOA/SURFACE}} = (F_a)_{\text{TOA/SURFACE}} - (F_{na})_{\text{TOA/SURFACE}} \quad (7)$$

where, F_a and F_{na} are the net radiative flux with aerosol and without aerosol conditions. Further, the amount of solar radiation absorbed by aerosols within the atmosphere ($\Delta F_{\text{ATM}} = \Delta F_{\text{TOA}} - \Delta F_{\text{SFC}}$) defines the net atmospheric forcing (ATM). If ΔF_{ATM} is positive, the aerosols produce a net gain of radiative flux in the atmosphere leading to a warming, while a negative ΔF_{ATM} indicates a net loss and thereby cooling.

The clear sky ADRF is estimated via SBDART model. The basic input parameters for the estimation of ADRF are spectral AOD, SSA, g, WVC, ozone concentration and surface albedo, along with astronomical parameters, like solar zenith angle. The spectral AOD, SSA, g and WVC were directly obtained from the sun/sky radiometer. In addition to the aerosol properties, the standard tropical atmospheric profiles (i.e. temperature, RH, pressure and ozone), from ECMWF reanalysis data and the MODIS (both Terra and Aqua) surface albedo (8-day, Level 3, Global 500 m SIN Grid product) at seven wavelengths (0.645, 0.859, 0.469, 0.555, 1.24, 1.64 and $2.13 \mu\text{m}$) are used in SBDART model (Dumka et al., 2014; Srivastava et al., 2014; Bisht et al., 2015; Tiwari et al., 2016). The ADRF calculations are performed using eight streams to obtain the TOA and surface upward and downward fluxes at every hour of a day with and without aerosols conditions in the wavelength range from $0.3\text{--}4.0 \mu\text{m}$. The diurnally averaged radiative forcing at TOA and surface is then obtained as the difference between net fluxes (down - up) with and without aerosols. The atmospheric heating rate (HR) due to absorption of solar radiation by aerosols in the atmosphere (net atmospheric forcing ΔF_{ATM}) is estimated from the first law of thermodynamics and hydrostatic equilibrium as:

$$\frac{\partial T}{\partial t} = \frac{g}{C_p} \times \frac{\Delta F_{\text{ATM}}}{\Delta P} \times 24 \left(\frac{\text{h}}{\text{day}} \right) \times 3600 \left(\frac{\text{s}}{\text{h}} \right) \quad (8)$$

where $\partial T/\partial t$ is the heating rate (K day^{-1}), g is the acceleration due to gravity, C_p is the specific heat capacity of air at constant pressure and ΔP is the atmospheric pressure difference between top and bottom boundaries of the atmosphere in which most of the aerosols occur and

is considered as 300 hPa (e.g. Kaskaoutis et al., 2013; Dumka et al., 2014).

3.6. Transport pathways

In order to understand the possible pathways and source identification of aerosol types and properties, seven-days air-mass back-trajectories over KVT are obtained from the HYSPLIT model (Draxler and Rolph, 2016) for the individual days of sun-photometer measurements. For the analysis, model is initiated with the 6 hourly Global Data Assimilation (GDAS) reanalysis fields at $1^\circ \times 1^\circ$. A clustering technique is used to classify different trajectories from various sources. The HYSPLIT model-simulated back trajectories are used to identify the general pathway of aerosol plume propagation and its evolution during autumn to spring (October–May). The trajectories are calculated at four times a day for the entire study period at three different heights (500 m-mixed layer height; 1000 m-boundary layer height and 2000 m-above the boundary layer where the aerosols can be lifted by convection and transported over long distances). The trajectory cluster analysis is performed to distinguish different aerosol transport pathways in the horizontal direction. Similar trajectories are paired to form clusters in the clustering analysis from which maximized differences are found. Further details of the clustering technique can be found in the references and the manual of the HYSPLIT model (Draxler and Rolph, 2016).

4. Results and discussion

4.1. Temporal variations of aerosols

AOD is representative of the aerosol burden in the atmospheric column, while α provides useful information on the aerosol size and constitutes. The temporal variability of instantaneous values of AOD_{500} , $\alpha_{440-870}$ and WVC are shown in Fig. 3. The blue line in the figure represents monthly mean values of AOD_{500} , $\alpha_{440-870}$ and WVC along with its standard deviation. The AOD_{500} ranges from ~0.06, corresponding to

clean-background conditions over KVT, up to ~1.5 or even ~2.3 on certain cases with severe aerosol loading in the atmosphere due to influence of dust storms, as those cases are associated with very low $\alpha_{440-870}$ values (<0.11). The large day to day variability in both AOD_{500} and $\alpha_{440-870}$ indicates the variability of aerosol types over the region due to transported air masses of different emission sources, either by long-range transport from Arabian Peninsula and Saharan or by advection from Indian subcontinents. The multi-annual variability shows a distinct behaviour of α with the large values (fine-mode aerosols) during November–February and low values during March–May (coarse-mode aerosols). Fig. 3 also reveals that the small variability in AOD_{500} and $\alpha_{440-870}$ from November to February corresponds to more homogenous atmospheric condition, while the large variability from March to May, indicating significant variations in air-mass origin and characteristics. The low AOD_{500} and $\alpha_{440-870}$ exist during October corresponding to wind-generated marine aerosols due to the extension of Indian summer monsoon (see Fig. 2), whereas the high AOD_{500} and $\alpha_{440-870}$ during winter season associated to transported anthropogenic pollution plumes and biomass-burning from Indian subcontinent. During the whole period, the mean values of AOD_{500} and $\alpha_{440-870}$ are found to be 0.51 ± 0.16 and 1.36 ± 0.3 , respectively. The annual distribution of climatological mean monthly WVC is shown in Fig. 3c, which exhibits a large seasonal variability. The WVC distribution showed a gradual decrease from October to February reaching minimum in February, thereafter gradually increase towards May. Strong westerlies/southwesterlies wind due to Indian summer monsoon carries a large amount of moisture from the oceanic region in May.

4.2. Climatology of aerosol properties

Fig. 4 shows the monthly variation of AOD values at three wavelengths (340,500 and 1020 nm), α value at three wavelength bands (440–870 nm, 440–670 nm and 670–870 nm) and WVC in Box-Whisker plots. The difference in α values between short and long-wavelengths defines the sign and magnitude of the curvature

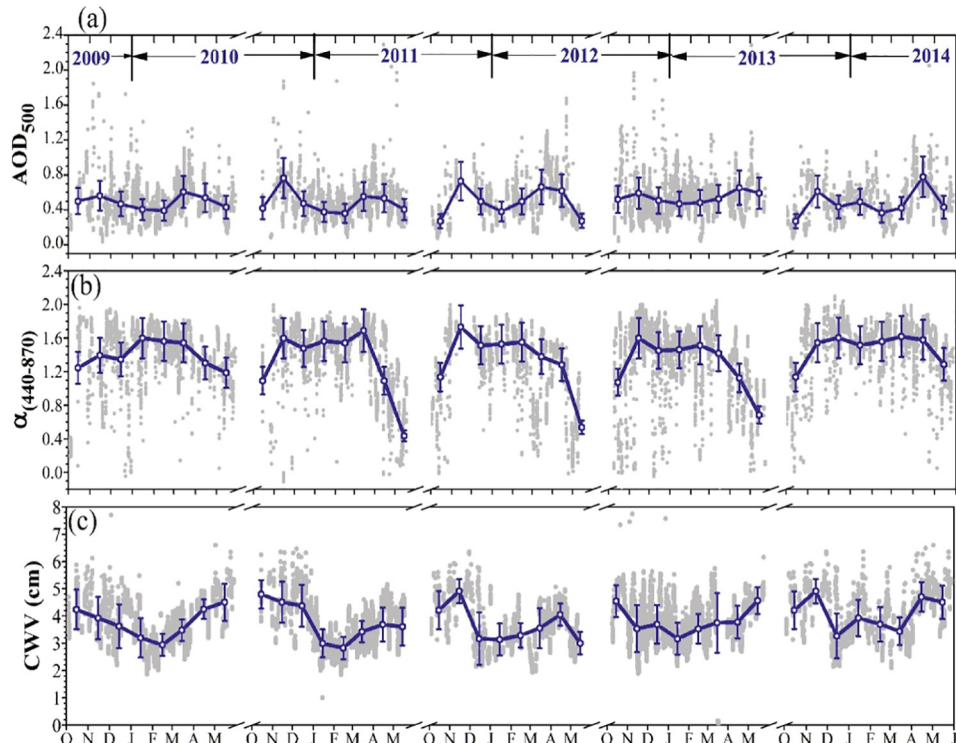


Fig. 3. The variation of instantaneous values of (a) aerosol optical depth at 500 nm (b) Ångström exponent at 440–870 nm and (c) columnar water vapor (in cm) in gray shade over KVT during the study period. The blue line represents the monthly mean values along with standard deviation. (For interpretation of the references to color in this figure legend, the reader is referred to the web version of this article.)

(Schuster et al., 2006), while inter-band variation of α values in short and long-wavelengths provides the information about the variation in fine-mode radii and fine-mode fraction, respectively. The monthly mean AOD shows a distinct pattern with decreasing tendency from October to February and it shows a pronounced increment in March. Subsequently, it has sudden fall from March to May, illustrating a bimodal AOD distribution with primary and secondary maxima in March and October, respectively. As expected, the AOD₃₄₀ is larger in all months compared to AOD₅₀₀ and AOD₁₀₂₀, while the significant monthly variation in the range of AOD at the particular wavelengths indicates more or less homogeneity in the aerosol burden. The large intra-monthly variability in aerosol burden exhibits in the October, March and April. The large range of Box for AOD₃₄₀ and AOD₁₀₂₀ in October gives a sign for large variability in the fine and coarse mode aerosols. Also, note that, throughout the year, the large range of AOD₃₄₀ box compare to AOD₅₀₀ and AOD₁₀₂₀ indicates the presence of fine mode aerosol burden in the atmospheric column, expressing the influence of continental anthropogenic aerosol from the Indian subcontinent. On seasonal basis, the AOD₅₀₀ is found to be 0.53 ± 0.20 , 0.45 ± 0.06 and 0.56 ± 0.17 in autumn, winter and spring, respectively.

The monthly mean distribution of α value (Fig. 4b) illustrates a definite increase from autumn to winter (~ 0.9 to 1.3), thenceforth gradually decrease during spring (~ 1.2 to 0.7). The lowest values of α during

April–May indicate a clear dominance of coarse-mode aerosols due to long-range transport of dust (Srivastava et al., 2014) along with marine aerosols (sea-salt) produced by the strong sea-surface winds over the Arabian Sea (Kaskaoutis et al., 2010; Patel and Shukla, 2015). The α values ~ 1.0 to ~ 1.2 during November–February reveals a rather mixing of fine and coarse mode aerosols (Eck et al., 2005). The similarity between $\alpha_{440-670}$ and $\alpha_{670-870}$ in November–February indicates a bimodal size distribution with lower curvature and nearly equal contributions by fine and coarse modes, while the larger values of $\alpha_{440-870}$ compared to $\alpha_{670-870}$ during April–May, suggest a positive curvature, indicating clear dominance of coarse particles (Schuster et al., 2006), as shown in Fig. 5. In general, the monthly pattern of α values follow the pattern of previous study carried out over Minicoy Island (Vinoj et al., 2010), while seasonal variability shows larger α values in winter 1.52 ± 0.08 , compared to autumn 1.33 ± 0.24 and spring 0.97 ± 0.39 . The WVC exhibits a similar pattern of AOD (Fig. 4c), with increasing values from winter to spring peaking at ~ 5.2 in May. This pattern of WVC is following the onset pattern of Indian summer monsoon.

4.3. Volume size distribution

The aerosol optical properties are strongly dependent on columnar size distribution, which is closely related to α , fine mode fraction and

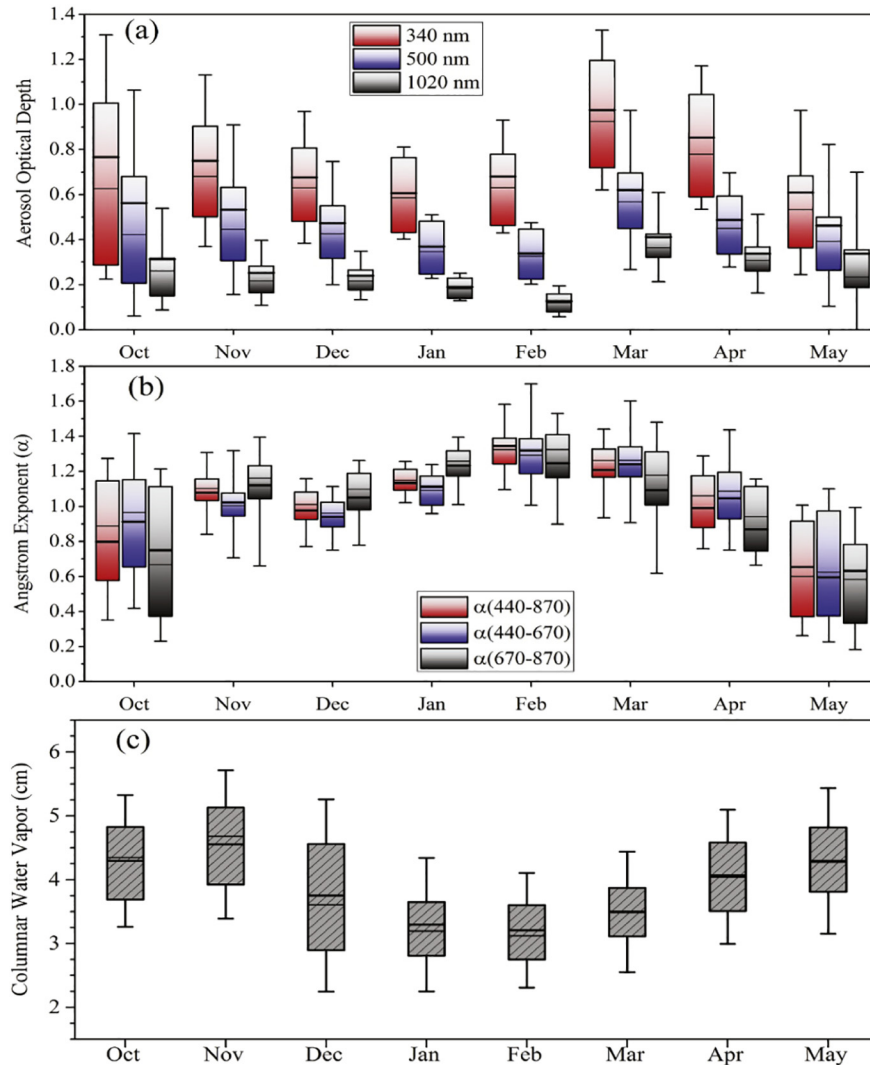


Fig. 4. Monthly mean distribution of (a) spectral aerosol optical depth at 340 nm, 500 nm and 1020 nm (b) Ångström wavelength exponent at three wavelength bands (440–870, 440–670 and 670–870 nm) and (c) water vapor content over KVT. Box-and-whisker plots denote the 95th and 5th percentiles, respectively. The box's upper, middle and lower limits are the 75th, 50th and 25th percentiles, the dark straight solid black line shows the mean value.

its variations (Eck et al., 2010; Sinha et al., 2012). Fig. 5(a)–(d) shows the monthly-mean and seasonal-mean of VSD over KVT, while the vertical bars correspond to one standard deviation from the mean. The overall uncertainty in the estimation of the VSDs is around 15% (Kaskaoutis et al., 2013). The monthly variability of VSD reveals a bimodal size distribution, which may depend on various factors e.g. growth of large particles by condensation of gas-phase reaction, mixing of two air masses (Hoppel et al., 1985), homogenous hetero-molecular nucleation and meteorological parameters. The size distribution reveals two distinct modes: fine (particle radii < 0.6 μm) and coarse (particle radii > 0.6 μm). The values of monthly mean variation in the parameters (volume concentration (V) and volume geometric radius (R_V)) of the bi-modal log-normal volume size distribution for each mode are shown in the Fig. 5. The volume geometric radius of fine mode particles is found to be large in the autumn and winter, indicating a coagulation of the anthropogenic aerosols, whereas the swelling of aerosols in the presence of abundant atmospheric water vapor (Fig. 4c) (Parameswaran and Vijayakumar, 1994) in the month of May, resulting the larger particles (~0.303), as seen in Fig. 5(c). On the contrary, the variation in volume geometric radius of coarse mode particles is found to be similar during the study period. This could be due to the influence of larger maritime aerosols (i.e. sea-salt) throughout the year. The large volume concentration of fine mode aerosol in the winter and coarse mode in the spring suggest the influence of continental anthropogenic aerosols from Indian subcontinent and long-range transport of dust from the Arabian Peninsula, respectively, that is reflected in α values at all wavelength bands (Fig. 4b). Although the fine and coarse-mode radius of VSDs do not change significantly between the months, the fine-to-coarse mode

fraction exhibits a pronounced variation, which affect the large variability of $\alpha_{675-870}$ between the months (Fig. 4b). The seasonal variability in VSDs (Fig. 5d) is characteristic of seasonally-changed air masses, aerosol properties and types and exhibits large similarities to the VSDs found over Kanpur (Singh et al., 2004; Kaskaoutis et al., 2013) and Delhi (Srivastava et al., 2014).

4.4. Single scattering albedo (SSA) and Asymmetry parameter (g)

SSA is one of the crucial aerosol properties that provide information about absorption/scattering nature of particles, which is defined as the ratio of scattering to total extinction (scattering + absorption) of solar radiation due to aerosols. Hypothetically, SSA has a unit value for purely scattering aerosols, like sulfate, and has low values for strongly absorbing aerosols, like soot/black carbon. The spectral variation of SSA gives useful information about the dominance of specific aerosol types (e.g. black carbon, organic carbon, dust, sulfates) and can also be used in combination with α and/or fine-mode fraction (FMF) for the identification of aerosol types (Srivastava et al., 2012, 2014). In the present study, the SSA is retrieved at four wavelengths (440, 675, 870 and 1020 nm) over KVT during October–May 2009–2014 and its seasonal mean-spectral variation is shown in Fig. 6(a). Spectral variation in SSA differs substantially during different seasons, depending on the relative proportions of absorbing and scattering components in the atmosphere. It shows an increasing trend with wavelength in spring due to influence of dust aerosol, which are highly scattering in visible and near-infrared region (Dubovik et al., 2002). In contrast, during autumn and winter, SSA is decreasing with increase in wavelength, indicating the

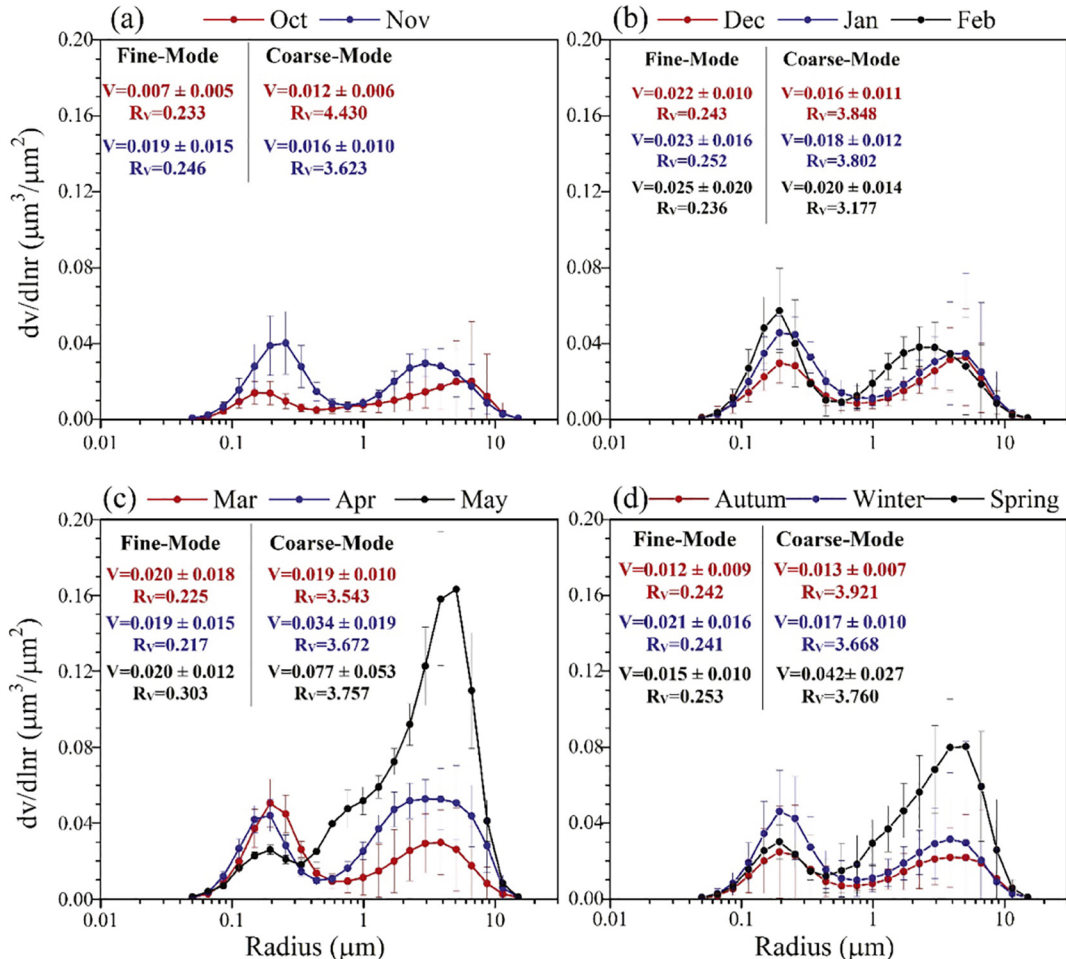


Fig. 5. (a–c) monthly and (d) seasonal trend of volume size distribution along with the values of volume concentration (V in $\mu\text{m}^3/\mu\text{m}^2$) and volume geometric radius (R_V in μm) for both fine and coarse mode particles over Kavaratti.

loading of absorbing polluted aerosols, as the interaction of these aerosols with the incoming solar radiation is minimum at longer wavelengths. Earlier study by Smirnov et al. (2002) in the Persian Gulf, also found a similar spectral variation of SSA, which indicate that the spectral behaviour of SSA depends on the nature of aerosol particles. In the spring (characterized by loading of dust), values of SSA are found higher, indicates more scattering particles, compared to the winter and autumn seasons, and characterized by a dominance of fine absorbing continental aerosols. Singh et al. (2004) also suggested that the increase in SSA during spring and summer may be also attributed to hygroscopic growth of water-soluble aerosols under high WVC besides the long-range transport of dust aerosols.

Asymmetry parameter (g) is the representation of the angular distribution of light scattering by aerosol particles and depends on the size and shape of the particle, which mainly controls the aerosols radiative forcing (Ramachandran and Rajesh, 2008; Tiwari et al., 2013). Asymmetry parameter can be defined by the cosine-weighted average of the scattering phase function (Pandithurai et al., 2008). Theoretically, the range of g varies between -1 (entirely backscattered light) to $+1$ (entirely forward scattered light). However, the zero value represents a pure symmetric scattering. Seasonal mean-spectral variation of g is shown in Fig. 6(b) over KVT. It shows a strong wavelength dependency in autumn and winter, which decrease with increase in wavelength. However, during spring, g increases in the near-infrared region, which can be attributed to the dominance of coarse-mode dust particles in the atmosphere. The sharp spectral decrease in g during autumn indicates the scattering by abundance of absorbing polluted aerosols, which further decreased from autumn to winter with increase in

absorbing aerosols. D'Almeida et al. (1991) suggested the g value of nearly 0.72 represents the fine-mode dry aerosol particles. Srivastava et al. (2011) found the g value 0.69 ± 0.02 over Kanpur. Recently, Tiwari et al. (2013) reported a value of 0.71 ± 0.02 over Karachi, 0.68 ± 0.02 over Lahore, 0.71 ± 0.01 over Jaipur, and 0.68 ± 0.02 over Kanpur during the pre-monsoon period. The results observed in the present study is somewhat similar to the several previous studies carried out over IGB (Pandithurai et al., 2008; Srivastava et al., 2011; Tiwari et al., 2013).

4.5. Identification of aerosol types

The characterization of aerosol types requires information on several optical and physical properties of aerosols that depend strongly on wavelength (e.g. Dubovik et al., 2002). The combined use of properties associated to aerosol loading and aerosol size is the most common and widely used technique for the discrimination different types of aerosol (Pace et al., 2006; Kaskaoutis et al., 2007, 2009; Yu et al., 2016; Patel and Kumar, 2015, 2016). The scatter plot of AOD vs. α is widely used method to classify variety of aerosol types. Fig. 7(a) shows such scatter plot using all instantaneous measurements over KVT. Furthermore, similar AOD vs. α graphs have been found over several sites in India, like Hyderabad (Kaskaoutis et al., 2009), Dehradun (Patel and Kumar, 2015), Pune (Vijayakumar and Devara, 2013), Jaipur (Verma et al., 2015) as well as over Arabian Sea (Kaskaoutis et al., 2010) and Bay of Bengal (Kaskaoutis et al., 2011). There is a wide range of $\alpha_{440-870}$ values for low-to-moderate AOD₅₀₀ suggesting large variability in the aerosol properties and several types of aerosol are mixed in the atmosphere over KVT. For quantifying the contribution of the major aerosol types, some threshold values are taken to discriminate the aerosol types, which are slightly deviated from the previous studies due to variation in the aerosol range, synoptic meteorological conditions, and the emission sources. More specifically, marine aerosol type (MA) representing the background conditions over KVT are considered as having AOD₅₀₀ < 0.3 and $\alpha_{440-870} < 0.9$, while clean continental (cc) aerosols are for AOD₅₀₀ < 0.3 and $\alpha_{440-870} > 1.0$. Cases corresponding to turbid atmospheres dominated by transported biomass burning aerosols or thick urban/industrial plumes (BB/UI) are for AOD₅₀₀ > 0.6 and $\alpha_{440-870} > 1.0$, while long-range transported desert dust (DD) aerosols are characterized by AOD₅₀₀ > 0.6 and $\alpha_{440-870} < 0.6$ (Fig. 7a). Cases that do not belong to any of the above categories are characterized as mixed type (MT) aerosols. Fig. 7(b) shows the total and seasonal percentage contribution of all five aerosol types at KVT. The MT are found to be dominate (~41%) over KVT with maximum in winter (~53%). In the same way, BB/UI aerosols is found to be second most contributor (~19%) with varying magnitude ranging from 16% to 23% and reaching maximum in winter (23%), rendering that KVT is strongly affected by the advected anthropogenically polluted aerosols from the Indian subcontinent. Indeed, the smoke plumes from the agricultural crop-residue burning in the southwest part of the Indian subcontinent are also influence the study region (Sahu et al., 2015). Earlier study by Ramachandran (2004) has also found about 90% anthropogenic contribution to the 5-yr (1996–2000) mean AOD over Arabian Sea. Furthermore, marine aerosols hold a significant fraction over the study region (17%) and contribute throughout the year as the background aerosols. Due to the neighbouring arid regions in west Asia that emit large amounts of dust in spring, the DD aerosols possess an important factor of 14% and peak in spring (~24%), while CC conditions over KVT are observed at 9% of the cases. It should be noted that the change in threshold values may be strongly modifying the percentages, therefore the discrimination must be considered only qualitatively not quantitative.

Furthermore, aerosol classification using spectral AAE and EAE has been widely used in recent times (Russell et al., 2010; Giles et al., 2011; and reference therein). Giles et al. (2011) characterized the absorbing aerosols in three major categories: mostly dust (where iron oxide in dust is dominant absorber), mostly BC (mixture of industrial

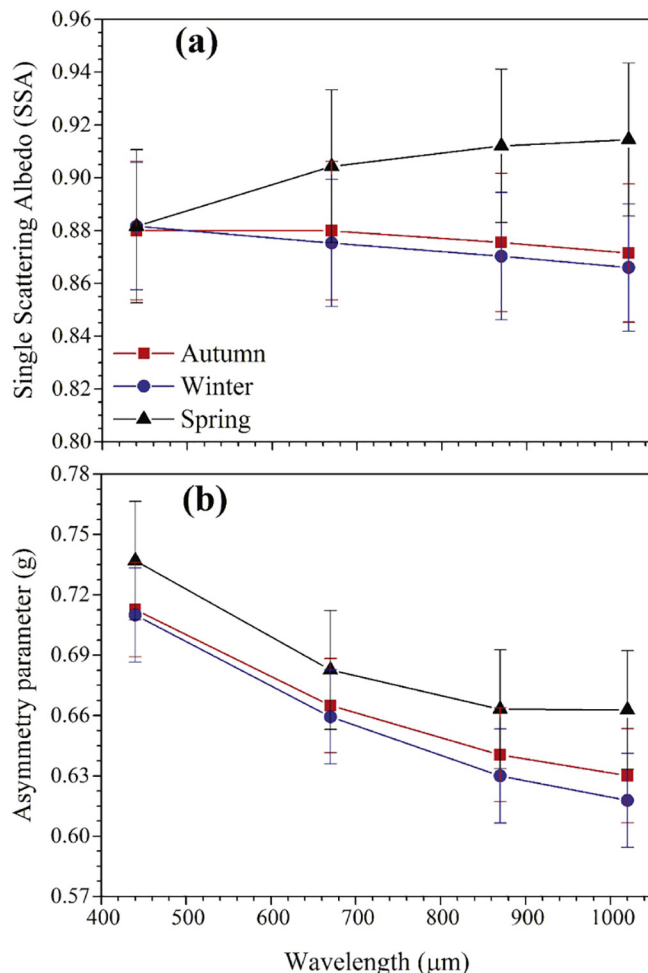


Fig. 6. Seasonal spectral variation of single scattering albedo and Asymmetry parameter.

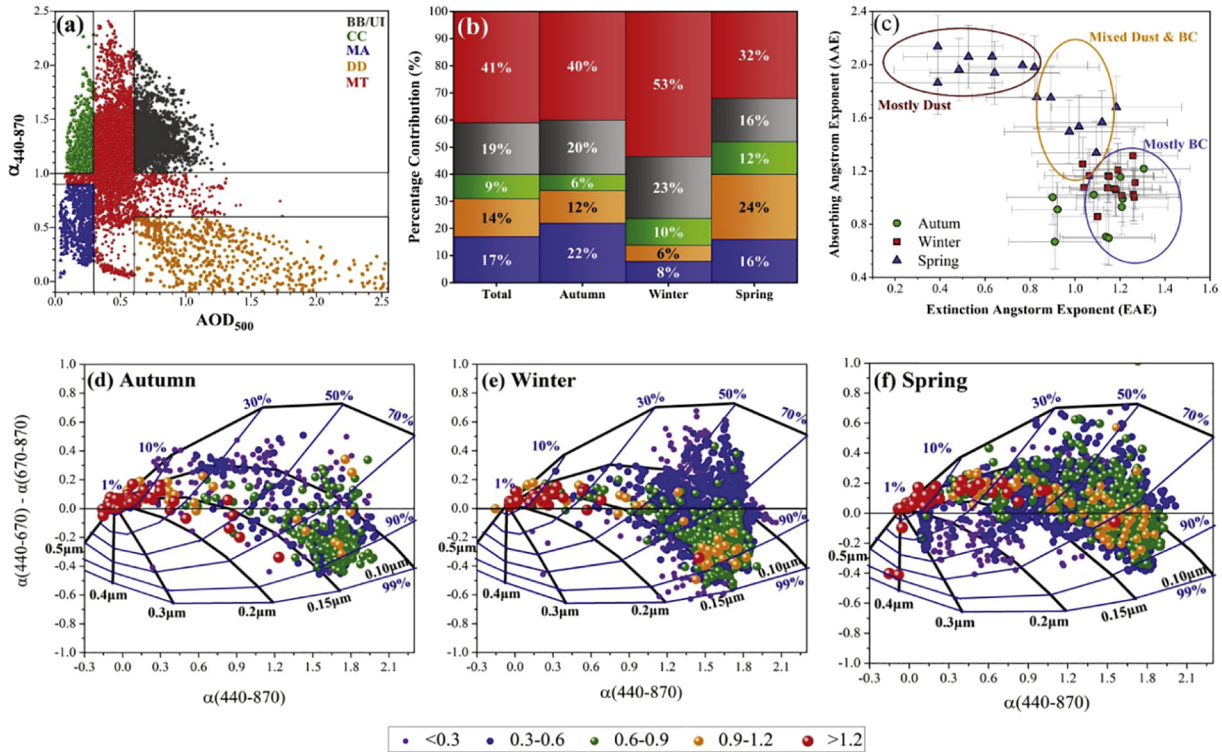


Fig. 7. (a) Scatter plot of AOD_{500} versus $\alpha_{440-870}$ with instantaneous data points identifying dominant aerosol types over KVT during the study period. (b) percentage of contribution of each aerosol type to the total. The label stand as BB/UI: biomass-burning aerosol or thick urban/industrial plumes, CC: continental conditions, MA: marine aerosol; DD: desert dust and MT: mixed type aerosols. (c) Monthly mean Absorption Ångström Exponent (AAE) as a function of Extinction Ångström Exponent (EAE) to identify the seasonal dominant aerosol type. (d-f) Ångström exponent difference, $d\alpha = \alpha_{(440-670 \text{ nm})} - \alpha_{(670-870 \text{ nm})}$, as a function of $\alpha_{(440-870 \text{ nm})}$ and AOD_{500} (color scale) over KVT for the autumn, winter and spring, respectively. The black lines indicate the fixed fine-mode radius (R_f) and the blue lines the fixed fine-mode fraction (η). Increase in the circle size denotes increase in AOD_{500} . (For interpretation of the references to color in this figure legend, the reader is referred to the web version of this article.)

pollution and biomass burning) and mixed dust and BC (optical mixture of coarse mode dust and fine mode BC as dominant absorber). The absorbing aerosols over KVT have been classified based on the above parameters into: Mostly Dust ($AAE > 1.8$, $EAE < 0.8$), Mostly BC ($0.8 < AAE < 1.4$, $EAE > 1.0$) and Mixed Dust and BC ($AAE \sim 1.5$, $EAE \sim 0.9$). The absorbing aerosols present over study location during autumn and winter are mostly BC and followed by the mixture of BC and Dust (Fig. 7c), however their contribution vary. During Spring, atmosphere over study location is characterized by presence of mixed BC and Dust absorbing aerosols, however the contributions of BC remains over the year at KVT, and significant during autumn and winter. It is observed that mostly dust aerosols are present during spring over KVT. The findings are pretty similar with Giles et al. (2011) and Kedia et al. (2014) over Kanpur, however their relative contribution vary.

In addition, the modification in aerosol properties over KVT is examined using the graphical scheme proposed by Gobbi et al. (2007), which combines the spectral information given by the determination of α in different spectral bands with the fine-mode radii (R_f) and fine-mode fraction (η) as grid parameters in grouped AOD. Therefore, the change in α , $d\alpha(\alpha_{440-670} - \alpha_{670-870})$ pairs with increasing AOD_{500} provides valuable information about several aerosol modification processes in the atmosphere (i.e. cloud contamination, hydration and coagulation-aging), as examined in a series of previous studies (e.g., Gobbi et al., 2007; Sinha et al., 2012; Kaskaoutis et al., 2010 and reference therein). In the present study (Fig. 7d-f), the aerosol modification processes are examined seasonally due to differing aerosol properties. A large variation is observed suggesting significant heterogeneity in the dominant particle sizes with a mixture of both fine and coarse mode particles. Negative $d\alpha$ indicates the dominance of fine-mode aerosols, while near zero or positive values correspond to bimodal size distribution with the coarse one to have a large fraction. A higher value of AOD_{500} occurred for fine mode particles (i.e. anthropogenic aerosols/biomass

burning) associated with increase in η ($>70\%$) with a larger AE difference and larger values of AE (>1.1) in winter. These are consistent throughout the period, and reaching maximum in winter, while a significant increase in R_f from $\sim 0.15 \mu\text{m}$ to $\sim 0.18 \mu\text{m}$ is also shown for these high-AOD data points, are linked to hygroscopic and/or coagulation growth from aging of the fine particles. Similar modifications were also found for aerosol over Hyderabad (Sinha et al., 2012), and over northern Bay of Bengal (Kaskaoutis et al., 2011) in autumn and winter, suggesting that such modification tend to be a general feature over India during the winter period with abundance of fine-anthropogenic aerosols. Fine-mode fraction below 30% occurs for moderate-to-low AODs over relative clean background marine regions due to the site location in the Arabian Sea. In contrast, during the spring, the vast majority of the data points exhibit η values $< 50\%$ or even $< 30\%$ and $\alpha_{440-870}$ usually below 0.8 suggesting clear dominance of coarse-mode aerosols (Fig. 7f). The shift in the data points towards the origin ($\alpha, d\alpha = 0$) with the increasing AOD, with R_f between ~ 0.10 – $0.13 \mu\text{m}$ and continuous decreasing values of η , suggesting a significant increase in coarse-mode fraction and a very small variation in fine-mode radii. The cases with $\eta < 30\%$ and R_f may increase to 0.2 – $0.4 \mu\text{m}$ indicating nearly absence of fine mode. These conditions are characteristics for environments strongly impacted by intense dust storms. Earlier studies over Arabian Sea (Kalapureddy and Devara, 2010; Kaskaoutis et al., 2010) have shown a similar feature.

4.6. Aerosol characterization inferred by absorption properties

The monthly mean spectral variation of AAOD in four wavelengths with AAE in three bands (440–875 nm, 675–870 nm and 440–675 nm) is shown in Fig. 8a, b, respectively. Both AAOD and AAE illustrate significant monthly variation over the study location. AAOD varies in the range of 0.058–0.091, 0.02–0.06, 0.012–0.046 and 0.01–0.045 for

440, 670, 870 and 1020 nm, respectively, whereas AAE varies within the range of 0.87–2.2, 0.9–1.95 and 0.5–1.65 for 440–870 nm, 440–670 nm and 670–870 nm bands, respectively. AAOD exhibits a similar monthly variation as the spectral AOD, it takes peak values in October, February and March, suggesting enhanced absorption either by biomass burning in October or by advected anthropogenically-polluted aerosols during winter (Fig. 8a). On the other hand, the larger values of AAOD correspond to dust and organic aerosols or mixes between them (AAE ~1.5) during April and May, which absorb strongly in the ultraviolet; AAE values ~1.0 reveal presence of BC aerosols, which show a strong absorption throughout the solar spectrum (Russell et al., 2010). Therefore, the larger values of AAE in the spring months indicate the absorption by dust mixed with other aerosols, in the shorter wavelengths, while the mixing of marine aerosols with dust may reduce the absorbing efficiency of dust, resulting in the lower value of AAE in May compare to April. The values of AAE ~1.0 during November–February suggest the significant contribution of absorbing aerosols, which are mainly composed by black carbon advected from India landmass (Vinoj et al., 2010).

Furthermore, we seasonally analysed the difference between SSA at 440 nm and 1020 nm ($dSSA = SSA_{1020\text{nm}} - SSA_{440\text{nm}}$) and correlated them with AAE in order to evaluate the absorbing aerosols and to associate their absorbing capability with the absorbing particle types. Moreover, a single parameter ($dSSA$) represents the spectral distribution of SSA, which is an advantage of this plot, and additionally, it provides better accuracy compare to absolute SSA values since the retrieval of spectral SSA dependence is more reliable than that of absolute values

(Derimian et al., 2008; Dumka et al., 2014). In this study, we also utilize the AAE, instead of AE, which can be used to distinguish between different sources of aerosols due to the differences in chemical composition that has an influence on aerosol light-absorption properties (e.g. Andreae and Gelencsér, 2006; Hoffer et al., 2006; Kirchstetter and Thatcher, 2012). The work by Moosmüller et al. (2011) provides a more in-depth view of its definition. The AAE close to 1 correspond to negative values of $dSSA$ will be related to strong absorption by BC containing particles at 1020 nm, while the $AAE > 1.8$ associated with positive values of $dSSA$ are related to stronger absorption by iron oxide (mineral dust) at 440 nm. Whereas, the AAE between 0.8 and 1.4 associated to nearly zero value of $dSSA$ will be related to equal contribution of BC and dust (mixed BC and dust). Fig. 8c, d illustrates the scatter plot and the density plot of $dSSA$ vs. AAE (440–870) over KVT, respectively. The gradual transition in the spectral SSA from stronger absorption at 1020 nm (negative $dSSA$) in autumn to stronger absorption at 440 nm (positive $dSSA$) in spring, which represents the heterogeneity of aerosol types and their chemical composition over KVT. The long-range transported dust in spring over study location increase the absorption at 440 nm, indicates the contamination of iron oxide, which shows the positive SSA with high value of AAE (>1.8). In contrast, negative SSA with AAE ~1 indicates the dominance of BC in the advected anthropogenically polluted particles from the Indian landmass in winter and having strong absorption at 1020 nm. There is absorption at both 440 nm and 1020 nm associated to nearly zero SSA value though out the study period, which could be attributed to the mixture of polluted aerosols

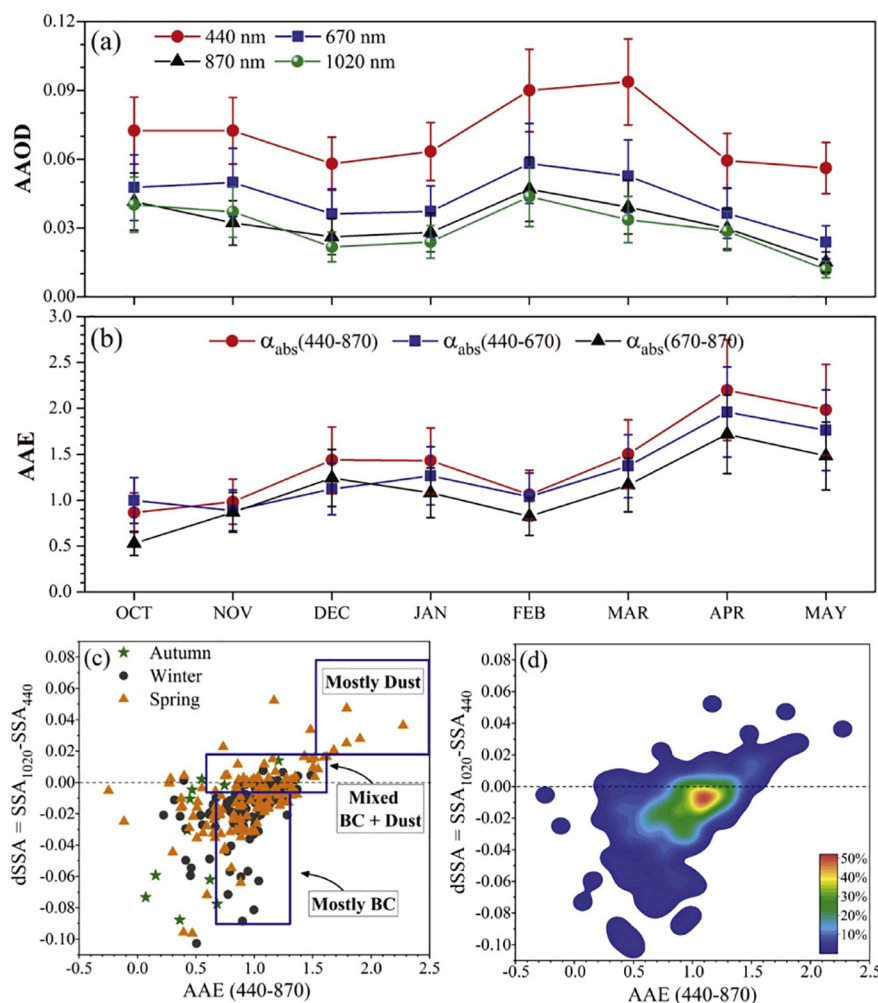


Fig. 8. Monthly mean distribution of (a) Absorbing aerosol optical depth (AAOD) at four wavelengths and (b) Absorbing Ångström Exponent (AAE) at three wavelength bands over KVT. The vertical bars correspond to one standard deviation from the monthly mean. Difference of SSA ($dSSA = SSA_{1020} - SSA_{440}$) versus AAE for (c) seasonal variation (d) percentage density.

with dust, having AAE from 0.8 to 1.4. Viewing the density plot (Fig. 8d) a clear-defined area of large density (~50%) is revealed for the dSSA, AAE pair of (~0.01, 1.1), which indicates, in the vast majority cases, the aerosol present over KVT are of mixed aerosols with a large fraction of BC contamination. Other secondary large density areas are those of (dSSA, AAE) of (~0.025, 1.0) corresponding to mostly BC containing fine-mode particles, having a strong absorption at 1020 nm. These analyses clearly indicate the influence of anthropogenic pollution transported from the Indian landmass to the remote island, throughout the study period, having potential to modify the regional climate and hydrological cycle.

4.7. Aerosol transport pathways

The preliminary knowledge of various aerosol types and their contributions is inferred from the analysis of inversion properties and aerosol type study over KVT. To know the source of these aerosols, their origin, the possible pathways and their percentage contribution, we performed the cluster analysis of HYSPLIT simulated backward trajectories over KVT. Fig. 9 shows the seasonal mean transport pathways and source regions of aerosols based on seven-days air-mass back trajectories

simulated by HYSPLIT model, ending over KVT at three altitudes (500 m, 1000 m and 2000 m above ground level), as described in Section 2.2. Polluted continental aerosols entrained from the Indian subcontinent to the study region during autumn to winter, whereas the transportation of dust from arid regions in the westwards dominates during spring. In depth, the trajectories during autumn are mostly from the Indian subcontinent (76%, 84% and 74% at 500 m, 1000 m and 2000 m, respectively) enriched with anthropogenic aerosols from urban areas, while a small fraction (~24%, 16%, and 26% at 500 m, 1000 m and 2000 m, respectively) corresponds to air masses coming from Northern Indian Ocean contains the marine signature (sea-salt). As a result, the 60% of AOD data are observed to be >0.5 with a high value of AE (>1.2) in winter. The subsequent transitions of air-mass pathways towards the arid regions in the Arabian Peninsula during spring, carries the dust as a large fraction of air-mass from long-range, which results increase in the coarse-mode volume concentration. The transportation of polluted air mass at 1000 m (~24%) and 2000 m (~35%) from east-side of the study location during spring, mixed with the dust, as seen in Fig. 8(c). The cluster analysis along with meteorological conditions suggests the monthly and seasonal variation in aerosol pathways that affect the local aerosol field.

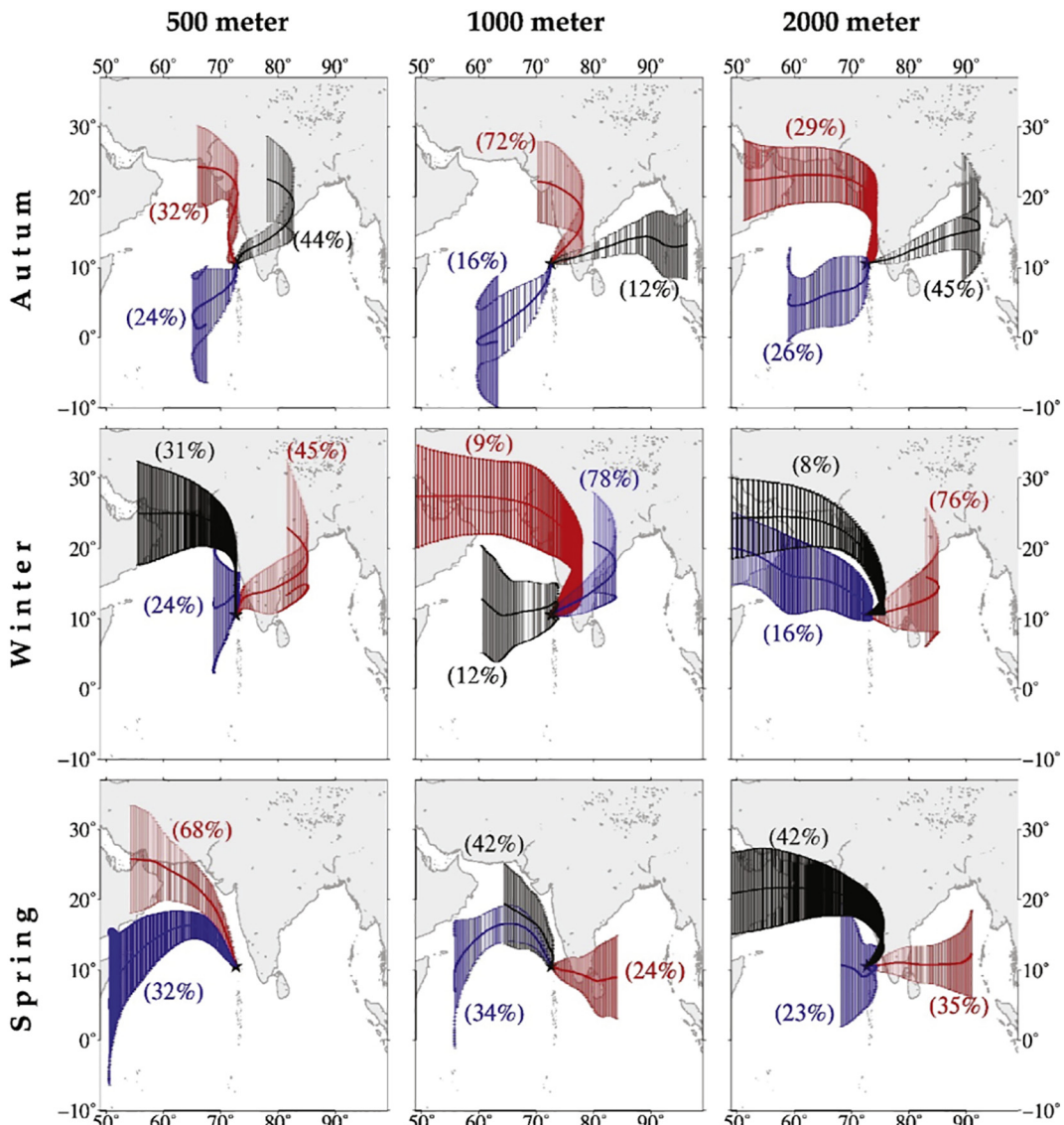


Fig. 9. Seasonal mean HYSPLIT model computed seven-days air mass back trajectory using cluster analysis at 500 m, 1000 m and 2000 m altitudes along with standard deviation during the study period over KVT.

4.8. Aerosol radiative forcing (ARF)

The ADRF at TOA, SFC and ATM are estimated on daily basis using the measured aerosol optical properties and SBDART model as described in Section 3.5. Fig. 10 summarizes the monthly variation of composite aerosol columnar radiative effects over KVT during the study period. The magnitude of ADRF at TOA, SFC and ATM exhibits significant variability between the months varying from -11.03 W m^{-2} (April) to -7.38 W m^{-2} (November) (mean: $-8.77 \pm 3.03 \text{ W m}^{-2}$) at TOA, while at SFC ADRF ranges from -21.52 W m^{-2} (April) to -14.33 W m^{-2} (December) (mean: $-16.71 \pm 5.22 \text{ W m}^{-2}$). The resultant ATM forcing ranges from 6.17 W m^{-2} (December) to 10.51 W m^{-2} (April) with a mean value of $7.94 \pm 2.76 \text{ W m}^{-2}$. The ADRF at SFC is a function of AOD₅₀₀, while the TOA ADRF depends strongly on SSA, and on the underlying surface albedo (Chand et al., 2009). Compared to TOA ADRF, the magnitude of ADRF at SFC is more fluctuating, which is relatively high in autumn, low in winter and high again in spring. An increase in AOD correlates the decrease in absorbing aerosols (e.g. BC; as seen in Fig. 7(b)) in spring, increased SSA and hence the SFC forcing. Conversely, the dominance of absorbing aerosols during winter decreases the values of SSA. The large difference in between TOA and surface ADRF exhibits that heating of the atmosphere due to absorption of solar radiation within the atmosphere, decreases eddy heat convergence, and induces a reduction in surface temperature (Ge et al., 2010). Moreover, the heating due to absorption of aerosol stabilizes close to its uppermost level at its maximum that may suppress the convective activity and present cloud formation (Koren et al., 2004). Translating the ADRF estimates to mean forcing efficiencies (forcing per unit AOD) are -17.27 W m^{-2} at TOA, -32.71 W m^{-2} at SFC with an average atmospheric forcing efficiency of $\sim 15.44 \text{ W m}^{-2}$, which is close to the value reported by Vinoj et al. (2010) for Minicoy island ($\sim 15 \text{ W m}^{-2}$). The low atmospheric absorption due to low BC mass fraction compared to Indian subcontinent resulting in the low atmospheric forcing over a remote island (Vinoj et al., 2010). Similarly, earlier studies over Arabian Sea (Vinoj and Satheesh, 2003; Moorthy et al., 2005) reported a low BC mass fraction over Arabian Sea compared to Indian subcontinent. The radiative and subsequently the climate implications of aerosols are assessed in terms of the atmospheric heating rate (Eq. (3)). The large value of heating rate in spring ($\sim 0.90 \text{ K day}^{-1}$) could possibly be due to the long-range transported dust from the Arabian Peninsula. This atmospheric heating in spring can have large implications for the regional climate, which can evaporate the low-level clouds resulting in a decrease in cloud cover and planetary albedo (Ackerman et al., 2000).

4.9. Vertical profile of aerosol and radiative forcing

Vertical profiles of aerosols are important and required for inferring the regional aerosol-induced climate perturbations. The dependence of vertical distribution becomes more important in view of aerosol absorption efficiency (Sathesh et al., 2010). Thus, the ADRF and HRs in the atmosphere are estimated based on the CALIPSO derived vertical profiles of the extinction coefficient over the study location, as discussed in Section 3.1. Fig. 11a shows the seasonal mean extinction profiles at 532 nm (average of day and night-time profile) over KVT. The observed CALIPSO extinction was found maximum near the surface ($0.32\text{--}0.44 \text{ km}^{-1}$) in all seasons that decreases significantly above 1 km heights, which are comparable to those observed over other urban conditions in India (Dumka et al., 2014; Sarangi et al., 2016 and reference therein). More specifically, the seasonal-mean extinction coefficient profiles are found larger ($>0.4 \text{ km}^{-1}$) near the surface in winter and autumn. In contrast, in spring, the profile of extinction coefficient reduces near the surface, while elevated layer of aerosol is evident between 2 and 5 km. Based on the seasonal-mean extinction profiles and assuming vertically homogenous SSA and g values (obtained from Sun/sky radiometer), the vertical profiles of atmospheric forcing (Fig. 11b) and HR (Fig. 11c) is estimated. The results revealed that the high atmospheric ADRF was found for level below 2 km during autumn and winter. In contrast, atmospheric forcing between 2 and 5 km during spring can be considered significant causing serious climate implications on the temperature gradients, onset, intensity and duration of monsoon and distribution of rainfall (Ramanathan et al., 2005; Gautam et al., 2009). The HR profiles obtained by inclusion of vertical profiles emphasizing the significant contribution of anthropogenic forcing near the surface in winter ($\sim 0.86 \text{ K day}^{-1}$) and autumn ($\sim 0.78 \text{ K day}^{-1}$), and the influence of dust at elevated layer (2–5 km) in spring ($\sim 0.3 \text{ K day}^{-1}$) over KVT. The fractional part of wind generated marine aerosols near the surface mixed with polluted aerosols may suppress the heating rate in autumn compare to winter over KVT, as seen in Fig. 7b. The observed HR profiles are lower than those observed over BoB (Moorthy et al., 2009), Delhi (Srivastava et al., 2012) and Kanpur, Bareilly and Nainital (Dumka et al., 2014). However, the standard deviations indicate the uncertainty involved in the profiles of ADRF and HR, since they are very much sensitive on the vertical distribution of aerosols. However, implementing all the uncertainties involved in the estimate of ADRF and HR profiles was found to be $\sim 12\text{--}15\%$ as discussed in Kaskaoutis et al. (2013), similar to that reported by other studies (Dey and Tripathi, 2008; Moorthy et al., 2009). However, it has been shown that the large surface cooling and atmospheric heating can affect the regional hydrological cycle

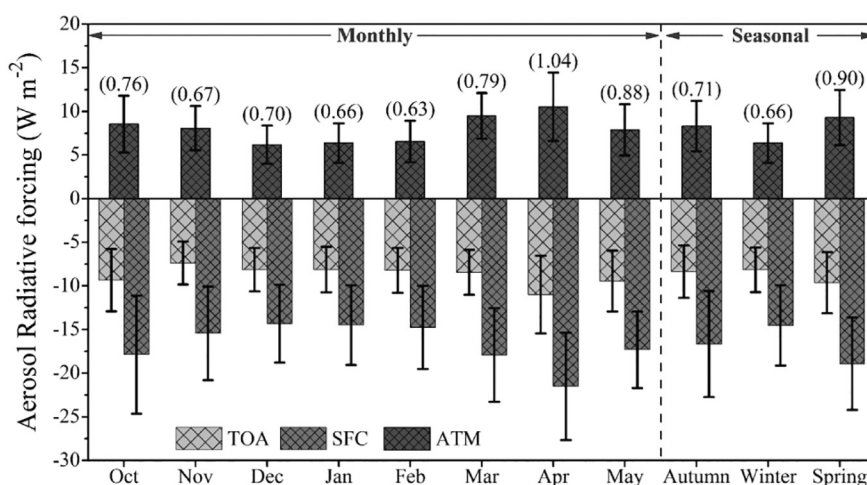


Fig. 10. Monthly and seasonal variation of aerosol radiative forcing at top-of-the-atmosphere (TOA), surface (SFC) and in the atmosphere (ATM). The values in brackets show the monthly mean heating rate.

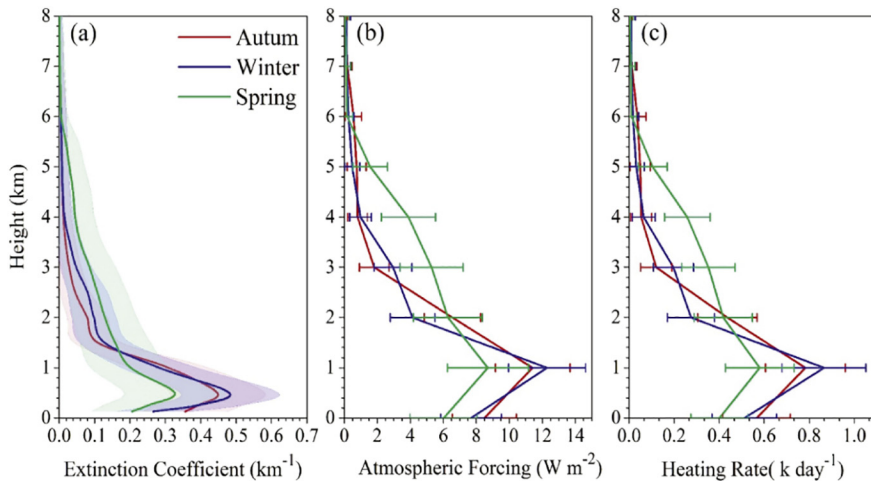


Fig. 11. Seasonal mean vertical profiles of (a) CALIPSO derived extinction coefficient, (b) atmospheric radiative forcing and (c) heating rate simulated using SBDART over KVT.

(Ramanathan et al., 2001b). This significant decrease in surface reaching solar radiation has important implications on the regional climate and monsoon circulations particularly in the context of the increasing trend of surface temperature (Kothawale and Rupa Kumar, 2005). To conclude this, the atmospheric warming near to surface and surface cooling may trap the upward (from Earth's surface to atmosphere) radiation (energy flow), resulting in the increase in low-level inversion and reinforce the boundary layer stability (Ackerman et al., 2000; Menon et al., 2002).

5. Conclusions

The present study analysed the aerosol optical and physical characteristics, aerosol type identification and radiative forcing over Kavaratti, Lakshadweep, a remote island located in the southern Arabian Sea from the period of observations (2009–2014) using ground-based sun/sky radiometer measurements. Changes in the microphysical properties of aerosols associated with the changes in the source impacts caused by changes in the advection pattern and their radiative implications are defined. The major findings are summarized below:

1. A significant variation in daily-mean values of AOD_{500} and $\alpha_{440-870}$ ranges from ~ 0.06 to 1.5 with annual means of 0.51 ± 0.16 and 1.36 ± 0.3 , respectively. On seasonal basis the AOD_{500} exhibits higher values in spring (0.56 ± 0.17) followed by autumn (0.53 ± 0.20) and winter (0.45 ± 0.06), while the low α values in spring (0.97 ± 0.39) indicate dominance of coarse-mode dust aerosols mixed with marine aerosols. Contrary, the higher α values in winter (1.52 ± 0.08) and autumn (1.33 ± 0.24) indicated the anthropogenic influence from Indian subcontinent.
2. The analysis of aerosol volume size distribution, SSA and g showed the aerosol field could be mostly characterized by the fine mode particles in autumn and winter, while the enhanced presence of dust in spring. The abundant atmospheric water vapor in late spring resulting in swelling of aerosols. The SSA was found to be significantly decrease with wavelength during autumn and winter (anthropogenically polluted aerosol), while it was increase with wavelength in spring (dust aerosols). The sharp spectral decrease in g during autumn and winter, indicate the scattering by loading of absorbing polluted aerosols, while it increased in the near-infrared region, which can be attributed to the dominance of dust in spring.
3. Aerosol type identification was attempted using the relationship between AOD_{500} and $\alpha_{440-870}$. The results revealed a dominance of the mixed type aerosols (~41%), with an important contribution of advected biomass-burning aerosols or thick urban/industrial plumes (~19%) and reaching maximum in winter (~53%), while marine aerosols contribute to 17%. Long-range transported desert dust

corresponded to 14% (maximum in spring (~24%)) of the cases, with the rest (~9%) correspond to continental conditions over Kavaratti.

4. A visualization scheme for scrutinizing the modification processes in the atmosphere, verified the previous findings, thus giving support to the accuracy of the retrievals and showed that increase in α during autumn and winter is related to fine-mode aerosol emissions and increase in fine-mode fraction, whereas the strong decrease in α in spring and clear dominance of aerosols from dust origin.
5. Aerosol characterization inferred by absorbing properties revealed the dominance of advected BC containing polluted particles from Indian subcontinent in winter, having strong absorption at 1020 nm, while abundance of iron oxide contained transported dust aerosol in spring increase the absorption at 440 nm with the large value of AAE (> 1.8). The large percentage density (~50%) correspond to the (dSSA, AAE) pair of (~0.01, 1.1), indicated the dominance of mixed aerosols with a large fraction of BC contamination over KVT.
6. The potential advection pathways have been identified by the trajectory cluster analysis. It has been observed that the fine mode anthropogenically polluted particles during winter are associated with continental air masses originated from the Indian subcontinent, while the spring coarse mode particles are mainly associated with air masses, which originated from arid regions of the Arabian Peninsula via Arabian Sea.
7. ADRF estimates over KVT were found to range from -11.00 W m^{-2} to -7.38 W m^{-2} and from -21.51 W m^{-2} to -14.33 W m^{-2} , at TOA and surface, respectively, with the atmospheric forcing varying between 3.17 W m^{-2} and 10.0 W m^{-2} resulting in atmospheric heating rates of $0.62\text{--}1.04 \text{ K day}^{-1}$. Additionally, the impact of aerosols on the vertical profiles of solar heating was much larger near surface in autumn and winter, while in spring, the heating rate was high between 2 and 4 km.

Acknowledgements

The authors gratefully acknowledge the constant encouragement received from the Director, SAC for carrying out the present research work. Valuable suggestions received from Deputy Director (EPSA) and Head (CVD) also gratefully acknowledged. We are thankful to the team members at Kavaratti Cal-Val site for data collection support. Authors also acknowledge the use of HYSPLIT model of NOAA-ARL for air mass back-trajectory analysis and MODIS for surface albedo data used in this paper. Authors would like to thank their respective families for their continuous motivations. The authors are grateful to anonymous reviewers for constructive and useful comments.

References

- Ackerman, A.S., Toon, O.B., Stevens, D.E., Heymsfield, A.J., Ramanathan, et al., 2000. Reduction of tropical cloudiness by soot. *Science* 288, 1042–1047.
- Andreae, M.O., Gelencser, A., 2006. Black carbon or brown carbon? The nature of light-absorbing carbonaceous aerosols. *Atmos. Chem. Phys.* 6:3131–3148. <http://dx.doi.org/10.5194/acp-6-3131-2006>.
- Ångström, A., 1964. The parameters of atmospheric turbidity. *Tellus* 16, 64–75.
- Babu, S.S., Moorthy, K.K., Satheesh, S.K., 2004. Aerosol black carbon over Arabian Sea during intermonsoon and summer monsoon seasons. *Geophys. Res. Lett.* 31, L06104. <http://dx.doi.org/10.1029/2003GL018716>.
- Beegum, S.N., Moorthy, K.K., Nair, V.S., Babu, S.S., Satheesh, S.K., Vinoj, V., Reddy, R.R., Gopal, K.R., Badarinath, K.V.S., Nirajan, K., Pandey, S.K., Behera, M., Jeyaram, A., Bhuyan, P.K., Gogoi, M.M., Singh, S., Pant, P., Dumka, U.C., Kant, Y., Kuniali, J.C., Singh, D., 2008. Characteristics of spectral aerosol optical depths over India during ICARB. *J. Earth Syst. Sci.* 117, 303–313.
- Beegum, S.N., Moorthy, K.K., Babu, S.S., Satheesh, S.K., Vinoj, V., Badarinath, K.V.S., et al., 2009. Spatial distribution of aerosol black carbon over India during pre-monsoon season. *Atmos. Environ.* 43, 1071–1078.
- Bergstrom, R.W., Pilewskie, P., Russell, P.B., Redemann, J., Bond, T.C., Quinn, P.K., Sierau, B., 2007. Spectral absorption properties of atmospheric aerosols. *Atmos. Chem. Phys.* 7: 5937–5943 (<http://www.atmos-chem-phys.net/7/5937/2007>).
- Bisht, D.S., Dumka, U.C., Kaskaoutis, D.G., Pipal, A.S., Srivastava, A.K., Soni, V., Attri, S.D., Sateesh, M., Tiwari, S., 2015. Carbonaceous aerosols and pollutants over Delhi urban environment: temporal evolution, source apportionment and radiative forcing. *Sci. Total Environ.* 521–522:431–445. <http://dx.doi.org/10.1016/j.scitotenv.2015.03.083>.
- Boucher, O., Randall, D., Artaxo, P., Bretherton, C., Feingold, G., Forster, P., Kermanen, V.M., Kondo, Y., Liao, H., Lohmann, U., Rasch, P., Satheesh, S.K., Sherwood, S., Stevens, B., Zhang, X.Y., 2013. Clouds and aerosols. In: Stocker, T.F., Qin, D., Plattner, G.-K., Tignor, M., Allen, S.K., Boschung, J., Nauels, A., Xia, Y., Bex, V., Midgley, P.M. (Eds.), Climate Change 2013: The Physical Science Basis. Contribution of Working Group II of the Fifth Assessment Report of the Intergovernmental Panel on Climate Change. Cambridge University Press, Cambridge, United Kingdom and New York, NY, USA.
- Campanelli, M., Nakajima, T., Olivieri, B., 2004. Determination of the solar calibration constant for a sun-sky radiometer: proposal of an in-situ procedure. *Appl. Opt.* 43, 651–659.
- Campanelli, M., Estellés, V., Tomasi, C., Nakajima, T., Malvestuto, V., Martínez-Lozano, J.A., 2007. Application of the SKYRAD improved Langley plot method for the in situ calibration of CIMEL sun-sky photometers. *Appl. Opt.* 46, 2688–2702.
- Chand, D., Wood, R., Anderson, T.L., Satheesh, S.K., Charlson, R.J., 2009. Satellite-derived direct radiative effect of aerosols dependent on cloud cover. *Nat. Geosci.* 2, 181–184.
- D'Almeida, G.A., Koepke, P., Shettle, E.P., 1991. Atmospheric Aerosols: Global Climatology and Radiative Characteristics. A. Deepak, Hampton.
- Derimian, Y., Karniel, A., Kaufman, Y.J., Andreae, M.O., Andreae, T.W., Dubovik, O., et al., 2008. The role of iron and black carbon in aerosol light absorption. *Atmos. Chem. Phys.* 8 (13):3623–3637. <http://dx.doi.org/10.5194/acp-8-3623-2008>.
- Dey, S., Di Girolamo, L., 2010. A climatology of aerosol optical and microphysical properties over the Indian subcontinent from 9 years (2000e2008) of Multiangle Imaging Spectroradiometer (MISR) data. *J. Geophys. Res.* 115, D15204. <http://dx.doi.org/10.1029/2009JD013395>.
- Dey, S., Tripathi, S.N., 2008. Aerosol direct radiative effects over Kanpur in the Indo-Gangetic basin, northern India: long-term (2001–2005) observations and implications to regional climate. *J. Geophys. Res.* 113, D04212. <http://dx.doi.org/10.1029/2007JD009029>.
- Draxler, R.R., Rolph, G.D., 2016. HYSPLIT (HYbrid Single-particle Lagrangian Integrated Trajectory) Model Access via NOAA ARL READY. NOAA Air Resources Laboratory, Silver Spring, MD. Website (<http://ready.arl.noaa.gov/HYSPLIT.php>).
- Dubovik, O., Holben, B.N., Eck, T.F., Smirnov, A., Kaufman, Y.J., King, M.D., Tanre, D., Slutsker, I., 2002. Variability of absorption and optical properties of key aerosol types observed in worldwide locations. *J. Atmos. Sci.* 59, 590–608.
- Dumka, U.C., Tripathi, S.N., Misra, A., Giles, D.M., Eck, T.F., Sagar, R., Holben, B.N., 2014. Latitudinal variation of aerosol properties from Indo-Gangetic plain to central Himalayan foothills during TIGERZ campaign. *J. Geophys. Res. Atmos.* 119. <http://dx.doi.org/10.1002/2013JD021040>.
- Eck, T.F., Holben, B.N., Reid, J.S., Dubovik, O., Smirnov, A., O'Neill, N.T., Slutsker, I., Kinne, S., 1999. Wavelength dependence of the optical depth of biomass burning, urban, and desert dust aerosols. *J. Geophys. Res.* 104 (D24):31,333–31,349. <http://dx.doi.org/10.1029/1999JD900923>.
- Eck, T.F., Holben, B.N., Dubovik, O., Smirnov, A., Glob, P., Chen, H.B., et al., 2005. Columnar aerosol optical properties at AERONET sites in central eastern Asia and aerosol transport to the tropical mid-Pacific. *J. Geophys. Res.* 110. <http://dx.doi.org/10.1029/2004JD005274>.
- Eck, T.F., et al., 2010. Climatological aspects of the optical properties of fine/coarse mode aerosol mixtures. *J. Geophys. Res.* 115, D19205. <http://dx.doi.org/10.1029/2010JD014002>.
- Estellés, V., Campanelli, M., Smyth, T.J., Utrillas, M.P., Martínez-Lozano, J.A., 2012. Evaluation of the new ESR network software for the retrieval of direct sun products from CIMEL CE 318 and PREDE POM01 sun-sky radiometers. *Atmos. Chem. Phys.* 12: 11619–11630. <http://dx.doi.org/10.5194/acp-12-11619-2012>.
- Gautam, R., Hsu, N.C., Lau, K.-M., Kafatos, M., 2009. Aerosol and rainfall variability over the Indian monsoon region: distributions, trends and coupling. *Ann. Geophys.* 29, 3691–3703.
- Ge, J.M., Su, J., Ackerman, T.P., Fu, Q., Huang, J.P., Shi, J.S., 2010. Dust aerosol optical properties retrieval and radiative forcing over north western China during the 2008 China-U.S. joint field experiment. *J. Geophys. Res.* 115, D00k12. <http://dx.doi.org/10.1029/2009JD013263>.
- Giles, D.M., Holben, B.N., Tripathi, S.N., Eck, T.F., et al., 2011. Aerosol properties over the Indo-Gangetic plain: a mesoscale perspective from the TIGERZ experiment. *J. Geophys. Res.* 116, D18203. <http://dx.doi.org/10.1029/2011JD015809>.
- Gobbi, G.P., Kaufman, Y.J., Koren, I., Eck, T.F., 2007. Classification of aerosol properties derived from AERONET direct sun data. *Atmos. Chem. Phys.* 7, 453–458.
- Haywood, J.M., Ramaswamy, V., Soden, B.J., 1999. Tropospheric aerosol climate forcing in clear-sky satellite observations over the oceans. *Science* 283, 1299–1303.
- Hoffer, A., Gelencser, A., Guyon, P., Kiss, G., Schmid, O., Frank, G.P., Artaxo, P., Andreae, M.O., 2006. Optical properties of humic-like substances (HULIS) in biomass-burning aerosols. *Atmos. Chem. Phys.* 6:3563–3570. <http://dx.doi.org/10.5194/acp-6-3563-2006>.
- Hoppel, W.A., Fitzgerald, J.W., Larson, R.E., 1985. Aerosol size distributions in air masses adverting off the east coast of the United States. *J. Geophys. Res.* 90, 2365–2379.
- IPCC: Intergovernmental Panel on Climate Change, 2007. Climate Change 2007: The Physical Science Basis Summary for Policymakers. 18(3). New York Cambridge University Press:pp. 433–440. <http://dx.doi.org/10.1260/095830507781076194>.
- Kalapureddy, M.C.R., Devara, P.C.S., 2010. Pre-monsoon aerosol optical properties and spatial distribution over the Arabian Sea during 2006. *Atmos. Res.* 95, 186–196.
- Kalapureddy, M.C.R., Kaskaoutis, D.G., Ernest Raj, P., Devara, P.C.S., Kambezidis, H.D., Kosmopoulos, P.G., Nastos, P.T., 2009. Identification of aerosol type over the Arabian Sea in the pre-monsoon season during the ICARB campaign. *J. Geophys. Res.* 114, D17203. <http://dx.doi.org/10.1029/2009JD011826>.
- Kaskaoutis, D.G., Kambezidis, H.D., 2006. Investigation on the wavelength dependence of the aerosol optical depth in the Athens area. *Q. J. R. Meteorol. Soc.* 132:2217–2234. <http://dx.doi.org/10.1256/qj.05.183/abstract>.
- Kaskaoutis, D.G., Kambezidis, H.D., Hatzianastassiou, N., Kosmopoulos, P.G., Badarinath, K.V.S., 2007. Aerosol climatology: on the discrimination of aerosol types over four AERONET sites. *Atmos. Chem. Phys. Discuss.* 7:6357–6411. <http://dx.doi.org/10.5194/acpd-7-6357-2007>.
- Kaskaoutis, D.G., Badarinath, K.V.S., Kharol, S.K., Sharma, A.R., Kambezidis, H.D., 2009. Variations in the aerosol optical properties and types over the tropical urban site of Hyderabad, India. *J. Geophys. Res.* 114, D22204. <http://dx.doi.org/10.1029/2009JD012423>.
- Kaskaoutis, D.G., Kalapureddy, M.C.R., Moorthy, K.K., Devara, P.C.S., Nastos, P.T., Kosmopoulos, P.G., Kambezidis, H.D., 2010. Heterogeneity in pre-monsoon aerosol types over the Arabian Sea deduced from shipboard measurements of spectral AODs. *Atmos. Chem. Phys.* 10, 4893–4908.
- Kaskaoutis, D.G., Kharol, S.K., Sinha, P.R., Singh, R.P., Kambezidis, H.D., Sharma, A.R., Badarinath, K.V.S., 2011. Extremely large anthropogenic-aerosol contribution to total aerosol load over the Bay of Bengal during winter season. *Atmos. Chem. Phys.* 11, 7097–7117.
- Kaskaoutis, D.G., Sinha, P.R., Vinoj, V., Kosmopoulos, P.G., Tripathi, S.N., Misra, A., Sharma, M., Singh, R.P., 2013. Aerosol properties and radiative forcing over Kanpur during severe aerosol loading conditions. *Atmos. Environ.* 79, 7–19.
- Kaskaoutis, D.G., Rashki, A., Francois, P., Dumka, U.C., Housos, E.E., Legrand, M., 2015. Meteorological regimes modulating dust outbreaks in southwest Asia: the role of pressure anomaly and inter-tropical convergence zone on the 1–3 July 2014 case. *Aeolian Res.* 18, 83–97.
- Kedia, S., Ramachandran, S., 2008a. Latitudinal and longitudinal variation in aerosol characteristics from sun photometer and MODIS over the Bay of Bengal and Arabian Sea during ICARB. *J. Earth Syst. Sci.* 117, 375–387.
- Kedia, S., Ramachandran, S., 2008b. Features of aerosol optical depths over the Bay of Bengal and the Arabian Sea during premonsoon season: variabilities and anthropogenic influence. *J. Geophys. Res.* 113, D11201. <http://dx.doi.org/10.1029/2007JD009070>.
- Kedia, S., Ramachandran, S., Holben, B.N., Tripathi, S.N., 2014. Quantification of aerosol type, and sources of aerosols over the Indo-Gangetic plain. *Atmos. Environ.* 98: 607–619. <http://dx.doi.org/10.1016/j.atmosenv.2014.09.022>.
- Kirchstetter, T.W., Thatcher, T.L., 2012. Contribution of organic carbon to wood smoke particulate matter absorption of solar radiation. *Atmos. Chem. Phys.* 12:6067–6072. <http://dx.doi.org/10.5194/acp-12-6067-2012>.
- Kobayashi, E., Uchiyama, A., Yamazaki, A., Kudo, R., 2010. Retrieval of aerosol optical properties based on the spheriod model. *J. Meteorol. Soc. Jpn.* 88, 847–856.
- Koren, I., Kaufman, Y.J., Remer, L.A., Martins, J.V., 2004. Measurement of the effect of Amazon smoke on inhibition of cloud formation. *Science* 303, 1342–1345.
- Kothawale, D.R., Rupa Kumar, K., 2005. On the recent changes in surface temperature trends over India. *Geophys. Res. Lett.* 32, L18714. <http://dx.doi.org/10.1029/2005GL023528>.
- Lawrence, M.G., Lelieveld, J., 2010. Atmospheric pollutant outflow from southern Asia: a review. *Atmos. Chem. Phys.* 10:11017–11096. <http://dx.doi.org/10.5194/acp-10-11017-2010>.
- Li, F., Ramanathan, V., 2002. Winter to summer monsoon variation of aerosol optical depth over the tropical Indian Ocean. *J. Geophys. Res.* 107:4284. <http://dx.doi.org/10.1029/2001JD000949>.
- Lodhi, N.K., Beegum, S.N., Singh, S., Kumar, K., 2013. Aerosol climatology at Delhi in the western Indo-Gangetic plain: microphysics, long-term trends, and source strengths. *J. Geophys. Res.* 118. <http://dx.doi.org/10.1029/jgrd.50165>.
- Menon, S., Hansen, J.E., Nazarenko, L., Luo, Y.F., 2002. Climate effects of black carbon aerosols in China and India. *Science* 297, 2249–2252.
- Mishra, M.K., Rajeev, K., Thampi, B.V., Parameswaran, K., Nair, A.K.M., 2010. Micropulse Lidar observations of mineral dust layer in the lower troposphere over the southwest coast of Peninsular India during the Asian summer monsoon season. *J. Atmos. Sol. Terr. Phys.* 72:1251–1259. <http://dx.doi.org/10.1016/j.jastp.2010.08.012>.
- Misra, A., Tripathi, S.N., Kaul, D.S., Welton, E., 2012. Study of MPLNET derived aerosol climatology over Kanpur, India, and validation of CALIPSO level 2 version 3 backscatter and extinction products. *J. Atmos. Ocean. Technol.* 29:1285–1294. <http://dx.doi.org/10.1175/JTECH-D-11-00162.1>.

- Moorthy, K.K., Satheesh, S.K., 2000. Characteristics of aerosols over a remote island, Minicoy in the Arabian Sea, optical properties and retrieved size characteristics. *Q. J. R. Meteorol. Soc.* 126, 81–109.
- Moorthy, K.K., Babu, S.S., Satheesh, S.K., 2003. Aerosol spectral optical depths over the Bay of Bengal: role of transport. *Geophys. Res. Lett.* 30:1249. <http://dx.doi.org/10.1029/2002GL016520>.
- Moorthy, K.K., Babu, S.S., Satheesh, S.K., 2005. Aerosol characteristics and radiative impacts over the Arabian Sea during the intermonsoon season: results from ARM field campaign. *J. Atmos. Sci.* 62:192–206. <http://dx.doi.org/10.1175/JAS-3378.1>.
- Moorthy, K.K., Satheesh, S.K., Suresh Babu, S.S., Dutt, C.B.S., 2008. Integrated campaign for aerosols, gases and radiation budget (ICARB): an overview. *J. Earth Syst. Sci.* 117: 243–262. <http://dx.doi.org/10.1007/s12040-008-0029-7>.
- Moorthy, K.K., Nair, V.S., Babu, S.S., Satheesh, S.K., 2009. Spatial and vertical heterogeneities in aerosol properties over oceanic regions around India: implications for radiative forcing. *Q. J. R. Meteorol. Soc.* 135, 2131–2145.
- Moorthy, K.K., Babu, S.S., Manoj, M.R., Satheesh, S.K., 2013. Build-up of aerosols over the Indian region. *Geophys. Res. Lett.* 40:1011–1014. <http://dx.doi.org/10.1002/grl.50165>.
- Moosmüller, H., Chakrabarty, R.K., Ehlers, K.M., Arnott, W.P., 2011. Absorption Ångström coefficient, brown carbon, and aerosols: basic concepts, bulk matter, and spherical particles. *Atmos. Chem. Phys.* 11:1217–1225. <http://dx.doi.org/10.5194/acp-11-1217-2011>.
- Nair, S.K., Parameswaran, K., Rajeev, K., 2005. Seven-years satellite observations of the mean structure and variabilities in the regional aerosol distribution over the oceanic areas around the Indian subcontinent. *Ann. Geophys.* 23, 2011–2030.
- Nakajima, T., Tonna, G., Rao, R., Boi, P., Kaufman, Y., Holben, B., 1996. Use of sky brightness measurements from ground for remote sensing of particulate polydispersions. *Appl. Opt.* 15, 2672–2686.
- Niranjan, K., Madhavan, B.L., Sreekanth, V., 2007. Micro pulse lidar observation of high altitude aerosol layers at Visakhapatnam located on the east coast of India. *Geophys. Res. Lett.* 34, L03815. <http://dx.doi.org/10.1029/2006GL028199>.
- Pace, G., di Sarra, A., Meloni, D., Piacentino, S., Chamard, P., 2006. *Aerosol optical properties at Lampedusa (central Mediterranean), 1. Influence of transport and identification of different aerosol types*. *Atmos. Chem. Phys.* 6, 697–713.
- Pandithurai, G., Dipu, S., Dani, K.K., Tiwari, S., Bisht, D.S., Devara, P.C.S., Pinker, R.T., 2008. Aerosol radiative forcing during dust events over New Delhi, India. *J. Geophys. Res.* 113, D13209. <http://dx.doi.org/10.1029/2008JD009804>.
- Parameswaran, K., Vijayakumar, G., 1994. Effect of atmospheric relative humidity on aerosol size distribution. *Indian J. Radio Space Phys.* 23, 175–188.
- Patel, P.N., Kumar, R., 2015. Estimation of aerosol characteristics and radiative forcing during dust events over Dehradun. *Aerosol Air Qual. Res.* 15:2082–2093. <http://dx.doi.org/10.4209/aaqr.2015.02.0077>.
- Patel, P.N., Kumar, R., 2016. Dust induced changes in ice cloud and cloud radiative forcing over a high altitude site. *Aerosol Air Qual. Res.* 16 (8):1820–1831. <http://dx.doi.org/10.4209/aaqr.2015.05.0325>.
- Patel, P., Shukla, A.K., 2015. *Aerosol optical properties over marine and continental sites of India during pre-monsoon season*. *Curr. Sci.* 108 (4), 666–676.
- Patel, P.N., Dumka, U.C., Kaskaoutis, D.G., Babu, K.N., Mathur, A.K., 2016. Optical and radiative properties of aerosols over Desalpar, a remote site in western India: source identification, modification processes and aerosol types discrimination. *Sci. Total Environ.* 575:612–627. <http://dx.doi.org/10.1016/j.scitotenv.2016.09.023>.
- Ramachandran, S., 2004. Spectral aerosol optical characteristics during the northeast monsoon over the Arabian Sea and the Tropical Indian Ocean: 2, Ångström and anthropogenic influence. *J. Geophys. Res.* 109, D19208. <http://dx.doi.org/10.1029/2003JD004483>.
- Ramachandran, S., Rajesh, T.A., 2008. Asymmetry parameters in the lower troposphere derived from aircraft measurements of aerosol scattering coefficients over tropical India. *J. Geophys. Res.* 113, D16212. <http://dx.doi.org/10.1029/2008JD009795>.
- Ramanathan, V., Crutzen, P.J., Lelieveld, J., Mitra, A.P., Althausen, D., Anderson, J., Andreae, M.O., Cantrill, W., Cass, G.R., Chung, C.E., Clarke, A.D., Coakley, J.A., Collins, W.D., Conant, W.C., Dulac, F., Heintzenberg, J., Heymsfield, A.J., Holben, B., Howell, S., Hudson, J., Jayaraman, A., Kiehl, J.T., Krishnamurti, T.N., Lubin, D., McFarquhar, G., Novakov, T., Ogren, J.A., Podgorny, I.A., Prather, K., Priestley, K., Prospero, J.M., Quinn, P.K., Rajeev, K., Rasch, P., Rupert, S., Sadourny, R., Satheesh, S.K., Shaw, G.E., Sheridan, P., Valero, F.P.J., 2001. Indian ocean experiment: an integrated analysis of the climate and the great Indo-Asian haze. *J. Geophys. Res.* 106, 28371–28398.
- Ramanathan, V., Chung, C., Kim, D., Bettge, T., Buja, L., Kiehl, J.T., Washington, W.M., Fu, Q., Sikka, D.R., Wild, M., 2005. Atmospheric brown clouds: impacts on South Asian climate and hydrological cycle. *PNAS* 102 (15):5326–5333. <http://dx.doi.org/10.1073/pnas.0500656102>.
- Ricchiazzi, P., Yang, S., Gautier, C., Sowle, D., 1998. SBDART: a research and teaching software tool for plane-parallel radiative transfer in the Earth's atmosphere. *Bull. Am. Meteorol. Soc.* 79, 2101–2114.
- Russell, P.B., Bergstrom, R.W., Shinozuka, Y., Clarke, A.D., De Carlo, P.F., Jimenez, J.L., Livingston, J.M., Redemann, J., et al., 2010. Absorption Ångström exponent in AERONET and related data as an indicator of aerosol composition. *Atmos. Chem. Phys.* 10, 1155–1169.
- Sahu, L.K., Sheel, V., Pandey, K., Yadav, R., Saxena, P., Guthe, S., 2015. Regional biomass-burning trends in India: analysis of satellite fire data. *J. Earth Syst. Sci.* 124 (7), 1377–1387.
- Sarangi, C., Tripathi, S.N., Mishra, A.K., Goel, A., Welton, E.J., 2016. Elevated aerosol layers and their radiative impact over Kanpur during monsoon onset period. *J. Geophys. Res. Atmos.* 121. <http://dx.doi.org/10.1002/2015JD024711>.
- Satheesh, S.K., Moorthy, K.K., 2000. *Aerosol characteristics over coastal regions of the Arabian Sea*. *Tellus* 49B, 417–428.
- Satheesh, S.K., Srinivasan, J., Moorthy, K.K., 2006a. Contribution of sea-salt to aerosol optical depth over the Arabian Sea derived from MODIS observations. *Geophys. Res. Lett.* 33, L03809. <http://dx.doi.org/10.1029/2005GL024856>.
- Satheesh, S.K., Moorthy, K.K., Kaufman, Y.J., Takemura, T., 2006b. Aerosol optical depth, physical properties and radiative forcing over the Arabian Sea. *Meteorog. Atmos. Phys.* 91:45–62. <http://dx.doi.org/10.1007/s00703-004-0097-4>.
- Satheesh, S.K., Vinoj, V., Moorthy, K.K., 2010. Radiative effects of aerosols at an urban location in southern India: observations versus model. *Atmos. Environ.* 44, 5295–5304.
- Schuster, G.L., Dubovik, O., Holben, B.N., 2006. Ångström exponent and bimodal aerosol size distributions. *J. Geophys. Res.* 111. <http://dx.doi.org/10.1029/2005JD006328>.
- Seinfeld, J.H., Pandis, S.N., 1997. *Atmospheric Chemistry and Physics: From Air Pollution to Climate Change*. John Wiley, Hoboken, N.J.
- Shukla, A.K., Babu, K.N., Prajapati, R.P., Suthar, N.M., Ajai, Sinha, A., Saifee, A.M., Satashia, S.N., Arul Muthiah, M., Venkatesan, R., 2013. An ocean CAL-VAL site at Kavaratti in Lakshadweep for vicarious calibration of OCM-2 and validation of geo-physical products - development & operationalization. *Mar. Geod.* 36, 203–218.
- Singh, R.P., Dey, S., Tripathi, S.N., Tare, V., Holben, B., 2004. Variability of aerosol parameters over Kanpur, northern India. *J. Geophys. Res.* 109, D23206. <http://dx.doi.org/10.1029/2004JD004966>.
- Sinha, P.R., Kaskaoutis, D.G., Manchanda, R.K., Sreenivasan, S., 2012. Characteristics of aerosols over Hyderabad in southern Peninsular India: synergy in the classification techniques. *Ann. Geophys.* 30:1393–1410. <http://dx.doi.org/10.5194/angeo-30-1393-2012>.
- Sinha, P.R., Dumka, U.C., Manchanda, R.K., Kaskaoutis, D.G., Sreenivasan, S., Moorthy, K.K., Babu, S.S., 2013. Contrasting aerosol characteristics and radiative forcing over Hyderabad, India due to seasonal mesoscale and synoptic-scale processes. *Q. J. R. Meteorol. Soc.* 139:434–450. <http://dx.doi.org/10.1002/qj.1963>.
- Smirnov, A., Holben, B.N., Eck, T.F., Dubovik, O., Slutsker, I., 2000. *Cloud screening and quality control algorithms for the AERONET database*. *Remote Sens. Environ.* 73, 337–349.
- Smirnov, A., Holben, B.N., Dubovik, O., O'Neill, N.T., Eck, T.F., Westphal, D.L., Goroch, A.K., Pietras, C., Slutsker, I., 2002. *Atmospheric aerosol optical properties in the Persian Gulf*. *J. Atmos. Sci.* 59, 620–634.
- Smirnov, A., Holben, B.N., Slutsker, I., et al., 2009. Maritime aerosol network as a component of aerosol robotic network. *J. Geophys. Res.* 114, D06204. <http://dx.doi.org/10.1029/2008JD011257>.
- Srivastava, R., Ramachandran, S., 2013. The mixing state of aerosols over the Indo-Gangetic plain and its impact on radiative forcing. *Q. J. R. Meteorol. Soc.* 139: 137–151. <http://dx.doi.org/10.1002/qj.1958>.
- Srivastava, A.K., Tiwari, S., Devara, P.C.S., Bisht, D.S., Srivastava, M.K., Tripathi, S.N., Goloub, P., Holben, B.N., 2011. Pre-monsoon aerosol characteristics over the Indo-Gangetic basin: implications to climatic impact. *Ann. Geophys.* 29, 789–804.
- Srivastava, A.K., Tripathi, S.N., Dey, S., Kanawade, V.P., Tiwari, S., 2012. Inferring aerosol types over the Indo-Gangetic Basin from ground based sun photometer measurements. *Atmos. Res.* 109–110, 64–75.
- Srivastava, A.K., Yadav, V., Pathak, V., Sachchidanand, Singh, Tiwari, S., Bisht, D.S., Goloub, P., 2014. Variability in radiative properties of major aerosol types: a year-long study over Delhi—an urban station in Indo-Gangetic Basin. *Sci. Total Environ.* 473–47: 659–666. <http://dx.doi.org/10.1016/j.scitotenv.2013.12.064>.
- Tiwari, S., Srivastava, A.K., Singh, A.K., 2013. Heterogeneity in pre-monsoon aerosol characteristics over the Indo-Gangetic basin. *Atmos. Environ.* 77, 738–747.
- Tiwari, S., Srivastava, A.K., Singh, A.K., Singh, S., 2015. Identification of aerosol types over Indo-Gangetic Basin: implications to optical properties and associated radiative forcing. *Environ. Sci. Pollut. Res.* <http://dx.doi.org/10.1007/s11356-015-4495-6>.
- Tiwari, S., Dumka, U.C., Kaskaoutis, D.G., Ram, K., Panicker, A.S., Srivastava, M.K., Tiwari, S., Attri, S.D., Soni, V.K., Pandey, A.K., 2016. Aerosol chemical characterization and role of carbonaceous aerosol on radiative effect over Varanasi in central Indo-Gangetic plain. *Atmos. Environ.* 125, 437–449.
- Verma, S., Prakash, D., Ricaud, P., Payra, S., Attié, J.L., Soni, M., 2015. A new classification of aerosol sources and types as measured over Jaipur, India. *Aerosol Air Qual. Res.* <http://dx.doi.org/10.2049/aaqr.2014.07.0143>.
- Vijayakumar, K., Devara, P.C.S., 2013. Study of aerosol optical depth, ozone, and precipitable water vapour content over Sinhagad, a high-altitude station in the Western Ghats. *Int. J. Remote Sens.* 34, 613–630.
- Vinoj, V., Satheesh, S.K., 2003. Measurements of aerosol optical depth over Arabian Sea during summer monsoon season. *Geophys. Res. Lett.* 30 (5):1263. <http://dx.doi.org/10.1029/2002GL016664>.
- Vinoj, V., Satheesh, S.K., Moorthy, K.K., 2008. *Aerosol characteristics at a remote island: Minicoy in southern Arabian Sea*. *J. Earth Syst. Sci.* 117, 389–397.
- Vinoj, V., Satheesh, S.K., Moorthy, K.K., 2010. Optical, radiative and source characteristics of aerosols at Minicoy, a remote island in the southern Arabian Sea. *J. Geophys. Res.* 115, D01201. <http://dx.doi.org/10.1029/2009JD011810>.
- Winker, D.M., Vaughan, M.A., Omar, A.H., Hu, Y., Powell, K.A., Liu, Z., Hunt, W.H., Young, S.A., 2009. Overview of the CALIPSO mission and CALIOP data processing algorithms. *J. Atmos. Ocean. Technol.* 26, 2310–2323.
- Yoon, J., Von Hoening-Huene, W., Kokhanovsky, A.A., Vountas, M., Burrows, J.P., 2012. Trend analysis of aerosol optical thickness and Ångström exponent derived from the global AERONET spectral observations. *Atmos. Meas. Tech.* 5:1271–1299. <http://dx.doi.org/10.5194/amt-5-1271-2012>.
- Yoon, J., Burrows, J.P., Vountas, M., Von Hoening-Huene, W., Chang, D.Y., Richter, A., Hilboll, A., 2014. *Changes in atmospheric aerosol loading retrieved from space-based measurements during the past decade*. *Atmos. Chem. Phys.* 14, 6881–6902.
- Young, S.A., Vaughan, M.A., 2009. The retrieval of profiles of particulate extinction from cloud aerosol Lidar and infrared pathfinder satellite observation (CALIPSO) data: algorithm description. *J. Atmos. Ocean. Technol.* 26:1105–1119. <http://dx.doi.org/10.1175/2008JTECHA1221.1>.
- Yu, X., Kumar, K.R., Lü, R., Ma, J., 2016. Changes in column aerosol optical properties during extreme haze-fog episodes in January 2013 over urban Beijing. *Environ. Pollut.* 210, 217–226.